The University of Southern Mississippi
The Aquila Digital Community

Master's Theses

Fall 2020

Assessing the Recalibration Interval for Nearshore Sediment Assemblages after Hurricane Irma: implications for Developing Long-term Records of Overwash Deposits

Stephen Mitchell

Follow this and additional works at: https://aquila.usm.edu/masters_theses

 Part of the Geology Commons, Oceanography Commons, and the Paleontology Commons

Recommended Citation

Mitchell, Stephen, "Assessing the Recalibration Interval for Nearshore Sediment Assemblages after Hurricane Irma: implications for Developing Long-term Records of Overwash Deposits" (2020). *Master's Theses*. 777.
https://aquila.usm.edu/masters_theses/777

This Masters Thesis is brought to you for free and open access by The Aquila Digital Community. It has been accepted for inclusion in Master's Theses by an authorized administrator of The Aquila Digital Community. For more information, please contact Joshua.Cromwell@usm.edu.

ASSESSING THE RECALIBRATION INTERVAL FOR NEARSHORE SEDIMENT ASSEMBLAGES AFTER HURRICANE IRMA: IMPLICATIONS FOR DEVELOPING LONG-TERM RECORDS OF OVERWASH DEPOSITS

by

Stephen Patrick Mitchell

A Thesis
Submitted to the Graduate School,
the College of Arts and Sciences
and the School of Ocean Science and Engineering
at The University of Southern Mississippi
in Partial Fulfillment of the Requirements
for the Degree of Master of Science

Approved by:

Dr. Davin Wallace, Committee Chair
Dr. Jessica Pilarczyk, Major Professor
Dr. Jeremy Deans

_____

Dr. Davin Wallace
Committee Chair

_____	_____	_____
Dr. Jessica Pilarczyk Major Professor	Dr. Robert J. Griffitt Director of School	Dr. Karen S. Coats Dean of the Graduate School

December 2020

COPYRIGHT BY

Stephen Patrick Mitchell

2020

Published by the Graduate School

ABSTRACT

Surface distributions are commonly collected to assist with overwash interpretation; however, many of these are first established immediately after a major overwash event as part of a post-event field survey. This study documents the impacts of Hurricane Irma, a Category 5 storm, on nearshore sediments off the coast of Anegada (British Virgin Islands) using distributions of *Homotrema rubra*, an encrusting foraminifer with a defined provenance in coral reef ecosystems. Over four sampling intervals spanning 2 years, from six months pre-Hurricane Irma to 18 months post-Hurricane Irma, surface sediment was collected from three shore-perpendicular transects on both the northern and southern shores of Anegada. Partitioning Around Medoids cluster analysis using the *Homotrema* data revealed that Hurricane Irma introduced an influx of well-preserved *fragments* into the reef flat (10% increase along the Windlass Bight transect and 13 % increase along the Soldier Point transect, the two northern transects) and homogenized the sediments, limiting the foraminifer's utility as a known sediment transport indicator. The homogenization of sediments along the two northern transects (i.e., reef proximal) persisted for 7-18 months, at which point *Homotrema* distributions returned to near pre-Hurricane Irma conditions. However, the southern transect (i.e., absence of reef), where *Homotrema* concentrations are significantly less, failed to recalibrate within the time period assessed by this study. Post-event recalibration intervals will vary based on site and event, however, our results suggest that a waiting period of at least 18 months is recommended before collecting surface sediment samples from nearshore environments offshore Anegada.

ACKNOWLEDGMENTS

We thank Sharleen DaBreo and the staff of the BVIs Department of Disaster Management for facilitating permits, granting access to field sites, and providing information regarding Hurricane Irma. Shirley Vanterpool from Anegada provided photos and eyewitness accounts of Hurricane Irma's landfall. Atoya George (BVI Conservation and Fisheries Department), Clayton Dike, Lillian Pearson, Tiffany Otai, and Brian Minkin assisted in fieldwork. This research was funded by the National Science Foundation (EAR-1801845), the United States Geological Survey Earthquake Hazards Program (G18AP00085), the Canadian Foundation for Innovation (CFI-JELF), the Canada Research Chair Program and an NSERC Discovery grant, and the German Research Foundation (DFG grant SP 1298/2-1). This work is a contribution to IGCP Project 639 "Sea Level Minutes to Millennia".

DEDICATION

I would like to take this time to thank some people for helping me in various ways during my time starting and completing this research. I would like to thank my friends and family for their encouragement, understanding, and support during this process. I would like to thank my lab mates Tiffany and Lillian as well as the other students involved in the USM Marine Science graduate program for their help and friendship. Lastly, I would like to thank Dr. Pilarczyk, who served as my mentor for the past four and a half years throughout both my undergraduate and graduate degrees and provided the funding for my graduate studies. Her guidance has taught me how to conduct research with integrity and attention to detail.

TABLE OF CONTENTS

LIST OF TABLES

LIST OF FIGURES

LIST OF ABBREVIATIONS

USM	The University of Southern Mississippi
PAM	Partitioning Around Medoids
BVIs	British Virgin Islands
WB	Windlass Bight
SP	Soldier Point
SS	South of Settlement

1. INTRODUCTION

Geological records of past land-falling storms and tsunamis provide insight into their patterns of timing and intensity as well as the spectrum of events that can be expected in the future (e.g., Sugawara et al., 2012; Toomey et al., 2013; Bregy et al., 2018). The 'proxy tool-kit' available to characterize and interpret overwash deposits in the geological record is ever expanding and includes proxies such as grain size (Donato et al., 2009; Hong et al., 2018), geochemistry (Moreira et al., 2017; Watanabe et al., 2020), and microfossils (Mamo et al., 2009; Pilarczyk et al., 2014a; Dura et al., 2016). Microfossils such as foraminifera are especially useful in understanding overwash patterns because they occupy both benthic and planktic marine environments, causing them to be entrained and transported landward during an overwash event (e.g., Mamo et al., 2009; Lane et al., 2011). In this respect, microfossils indicate the origin, or provenance, of the sediments deposited by storms and tsunamis (Hippensteel and Martin 1999; Lane et al., 2011; Kosciuch et al., 2018) and can assist in tracing the inland extent of past overwash events (e.g., Pilarczyk et al., 2012).

While microfossils have been used with great success in overwash studies (e.g., Mamo et al., 2009; Pilarczyk et al., 2014a), their utility as indicators of paleo-overwash is limited by the lack of regional surface distribution studies that document baseline conditions and serve as a basis for comparison with overwash deposits preserved within the geological record (e.g., Mamo et al., 2009). Surface distribution studies document the specific microfossil assemblages of coastal, nearshore and offshore environments (e.g., Strotz et al., 2016; Pham et al., 2018; Culver et al., 2019; Pilarczyk et al., 2020), which can often be different than the broad-scale ecological niches described in atlases that

cover larger areas (e.g., Debenay 2012; Loeblich and Tappan 1987). Often times, the first documentation of surface distributions are collected during post-event field surveys (Pilarczyk et al., 2012; Kosciuch et al., 2018) even though it is unclear the impact overwash processes have on the distributions and concentrations within microfossil assemblages of coastal and nearshore environments.

In this study we assess changes in the nearshore distributions of *Homotrema* rubra (foraminifer common in tropical reef environments) at Anegada, British Virgin Islands (BVIs) before and after Hurricane Irma (Category 5) impacted the island on 6th September 2017. *Homotrema rubra* has a defined provenance and becomes detached by waves, at which point it predictably bleaches from red to white as a result of exposure to ultraviolet light (MacKenzie et al., 1965; Phalen et al., 2016). *Homotrema's* defined provenance and predictable pattern of bleaching of *Homotrema* make it useful as a sediment transport indicator (MacKenzie et al., 1965; Pilarczyk et al., 2014b; Alam et al., 2018). Owing to its utility as an indicator of sediment provenance and transport, *Homotrema* has also been used to document overwash sediments (Pilarczyk and Reinhardt, 2012). The aim of this study is to assess the changes within surface *Homotrema* assemblages at Anegada, BVIs as a result of a major storm to determine the time interval required for these assemblages to return to pre-storm conditions. The results of this study are relevant for overwash research as they document both the disturbance and recovery of the coast and associated habitats after an intense (Category 5) hurricane.

2. REGIONAL SETTING

Anegada, BVIs is a 54 km^2 microtidal (< 0.5 m) island that is among the most low-lying (8 m above mean sea level; Atwater et al., 2012; 2014) in the Caribbean (Fig. 1). Prominent geomorphological features on Anegada include a series of shallow hypersaline ponds that are situated within a few tens to hundred of meters from the shoreline, as well as dune ridges on the north side of the island that reach approximately 2 m above sea level, and a relatively flat interior characterized by a weathered limestone surface that resembles a former carbonate platform (Atwater et al., 2012; 2014).

Anegada's northern coast directly faces the Puerto Rico Trench, placing Anegada at risk of inundation from near-field tsunamis (e.g., Zahibo et al., 2003; Atwater et al., 2017). Far-field tsunamis, such as the 1755 Lisbon event, also pose risk of inundation to Anegada (Atwater et al., 2012; 2014). Similarly, the island faces the open Atlantic and is situated in an area that has been impacted by frequent hurricanes (Schomburgk 1832; Dunn et al., 1961; Millás and Pardue 1968; Pickering 1983; Spiske et al., 2014). Notable hurricanes in recent times include: Hurricane Donna in 1960 (Category 3), Hurricane Hugo in 1989 (Category 5), Hurricane Earl in 2010 (Category 4), and most recently, Hurricane Irma in 2017 (Category 5).

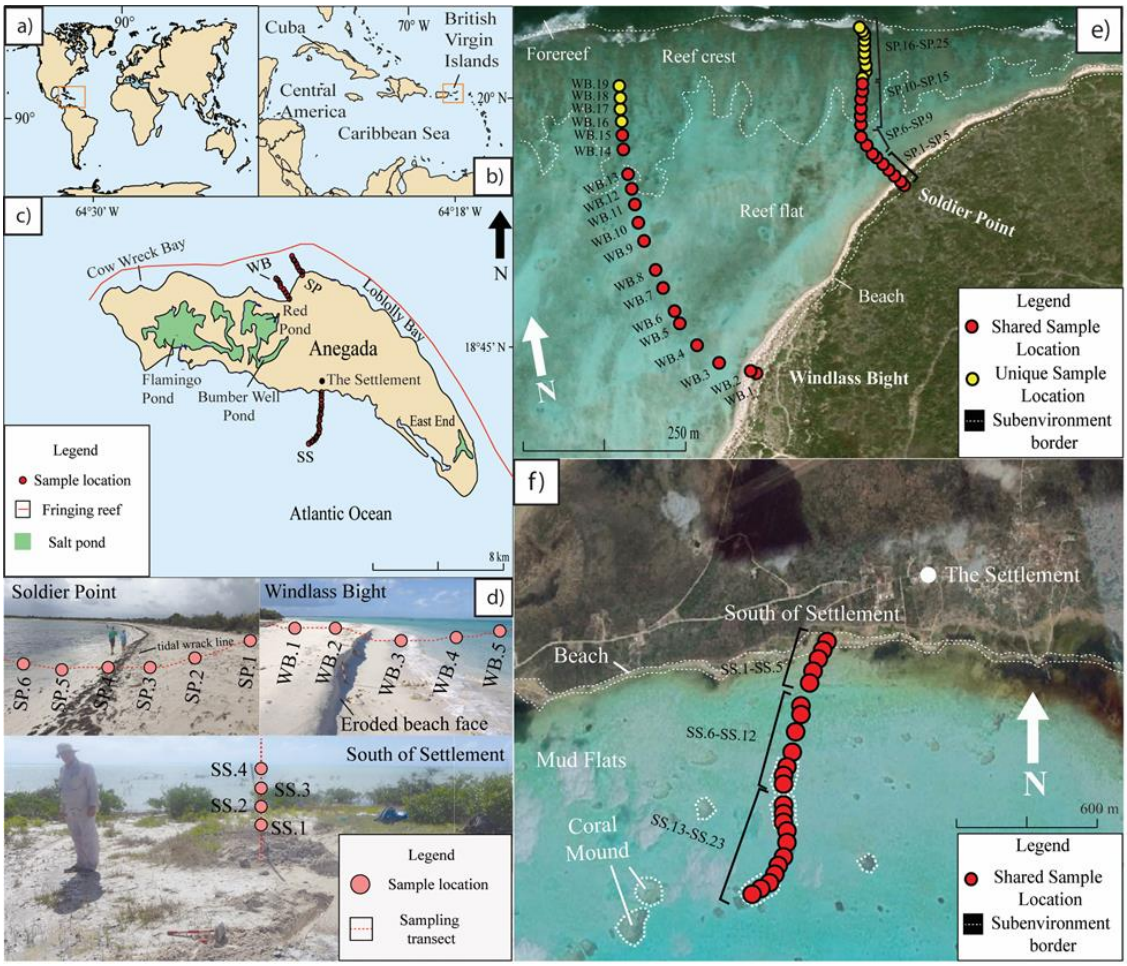

Figure 1*: Site Map*

Global (a) and regional (b) location map of the study site (red-outlined box). (c) Site map of Anegada, BVIs showing surface sample locations (red circles) along transects WB, SP, and SS. (d) Photos of the onshore sampling sites at Windlass Bight, Soldier Point, and South of Settlement. Detailed maps of the study site on the northern (e) and southern (f) shores of Anegada showing broad-scale geomorphologic features. Red circles indicate locations that were sampled at multiple intervals pre- and post-Hurricane Irma, while yellow circles indicate locations that were not shared among the pre- and post-Irma sampling transects.

Hurricane Irma began as a tropical depression west of Cape Verde on 30th August 2017, intensifying to Category 1 status one day later. Over the next 5 days Hurricane Irma rapidly intensified into a Category 5 storm as it tracked towards the northern Leeward islands with maximum sustained winds of 285 km/h (Cangialosi et al., 2018). The storm's first landfall in the Caribbean was on Barbuda, where windspeeds reached

296 km/h and a 2.4 m storm surge was recorded (Cangialosi et al., 2018). In the early afternoon of 6th of September 2017, Irma's eye passed approximately 35 kilometers south of the island of Anegada as a Category 5 with windspeeds reaching 287 km/h. As Hurricane Irma passed Anegada on track towards Cuba, it produced wind speeds up to 268 km/h and a resulting 2.0 m storm surge. As the system tracked northeast it weakened to a Category 3 before making landfall on Florida on 10th September 2017 with wind speeds of 185 km/h and a resulting storm surge of 1.5-2.5 m in the Keys (So et al., 2019). The storm continued to weaken as it moved north into Florida and was downgraded to a tropical storm status on 11th September 2017 (Cangialosi et al., 2018).

Storm surge data for the BVIs is limited as a result of malfunctioning or destroyed tide gauges due to the strong winds during the storm (Cangialosi et al., 2018). Hurricane Irma caused significant damage in the BVIs that persisted for months after the storm impacted the island (e.g., destroyed homes and roadways, and lack of access to electricity). A post-event field survey conducted at Anegada in January 2018 found that "substantial coastal erosion occurred on Anegada's north shore where the surge reached about 3.8 meters above sea level and had an onshore flow depth of up to 1.6 meters" (Spiske et al., in prep). While overwash deposition was reported on the northern, eastern, and southern shores of the island, Hurricane Irma's storm surge caused significant erosion on the northwest side (Spiske et al., in progress).

3. METHODS

3.1 Field sampling

Three main sites were targeted for surface sediment sampling: Windlass Bight (WB; north side of the island), Soldier Point (SP; north side of the island), and South of Settlement (SS; south side of the island; Fig. 1). Transects WB, SP, and SS were established (Fig. 1d-f) and spanned major point sources of sediment available for transport by storm surge: dunes, beach, reef/mud flat, and reef crest. Of the three transects, two were established on the north side of the island (WB and SP) to assess the spatial variability in *Homotrema* assemblages over a short distance (525 m between separate transects WB and SP). The third transect was established on the south side of the island (SS) so that differences in *Homotrema* assemblages between the northern (major source of *Homotrema* due to the presence of a fringing reef) and the southern (negligible source of *Homotrema* due to absence of a reef) sides of the island could be assessed.

Each transect was resampled three to four times over the course of 24 months to capture changes as a result of Hurricane Irma's storm surge. Sampling intervals include March 2017 (6 months before Hurricane Irma impacted Anegada), January 2018 (4 months after Irma), August 2018 (11 months after Irma) and March 2019 (18 months after Irma) (Fig. 2). The northern transects (WB and SP) were only sampled at three intervals due to inclement weather and unsafe water conditions. As a result, WB was sampled in March 2017, January 2018, and August 2018, and SP was sampled in March 2017, January 2018, and March 2019. SS was sampled in in each of the four sampling intervals (Fig. 2).

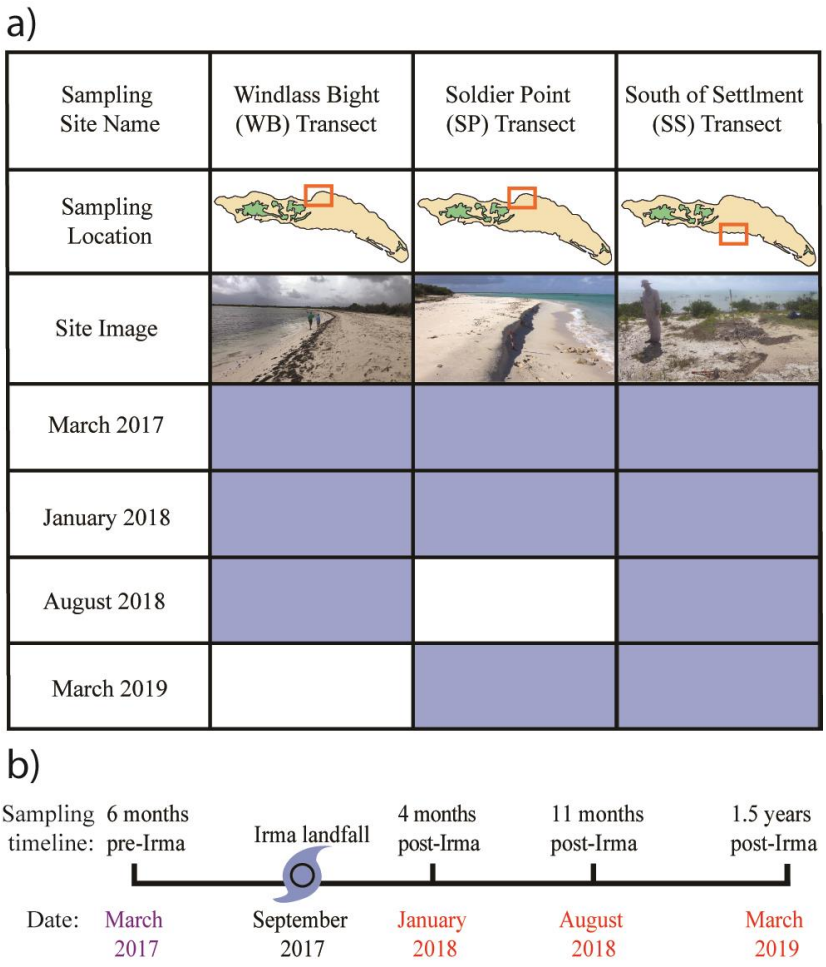

Figure 2: *Sampling strategy*

Sampling strategy (location and collection interval) for Windlass Bight (WB), Soldier Point (SP), and South of Settlement (SS) transects. (a) Sampling intervals for all three transects. Blue shading indicates a sampled interval. (b) Sampling timeline before and after Hurricane Irma.

A total of 240 collection sites were sampled for surface sediments along the three transects (62 from WB, 66 from SP, and 112 from SS). Sampling involved collecting the upper 1-2 cm of surface sediment from the reef tract using 50 mL centrifuge tubes. At key inflection points (i.e., change in water depth or noticeable environmental change), samples were collected by wading out and/or free diving along the reef tract. At each sample site we recorded the water depth using a handheld Hondex digital depth sounder

and recorded the location using a handheld Garmin GPS. Samples were refrigerated at 2 - 4°C until they were prepared for microfossil analysis.

3.2 Microfossil analysis

Owing to its defined provenance in the reef (Phalen et al., 2016) and its proven utility as a sediment transport indicator (MacKenzie et al., 1965; Machado and Moraes, 2002; Pilarczyk et al., 2014b; Alam et al., 2018), distributions of *Homotrema* rubra were isolated from the full foraminiferal assemblage following the methods of Pilarczyk and Reinhardt (2012).

Prior to analysis under the microscope, ~5 cm^3 of sediment from each sample was subsampled and wet sieved using a 45 μm mesh. Samples were then placed in a drying oven at 35°C for 24 hours, at which point, samples were split into fractions using a microsplitter to concentrate approximately 300 individuals per subsample (Scott and Hermelin, 1993). Once split into aliquots, the dried samples were sieved into different size fractions using the following categories: >500 μm, 500- 250 μm, 250-150 μm, and <150 μm. *Homotrema* fragments in each size fraction were then examined using an Olympus SZX16 stereomicroscope to determine their taphonomic condition. Each *Homotrema* fragment was categorized into one of four possible taphonomic categories based on Pilarczyk and Reinhardt (2012): exceptionally preserved (bright red in color, angularly shaped, intact chambers), well-preserved (pink in color, angularly shaped, hollowed out chambers), moderately preserved (light pink in color, slightly rounded shape, smoothed out chambers), and highly altered (very light pink to white in color, rounded shape, smoothed out chambers) (Fig. 3). Total concentration of *Homotrema* fragments (number of specimens per cm^3), taphonomic condition (% relative abundance), and test size (%

relative abundance) were calculated for each sample (Table S1) and plotted against increasing distance from the shoreline (Figs. 4-6; Figs. S1-S3).

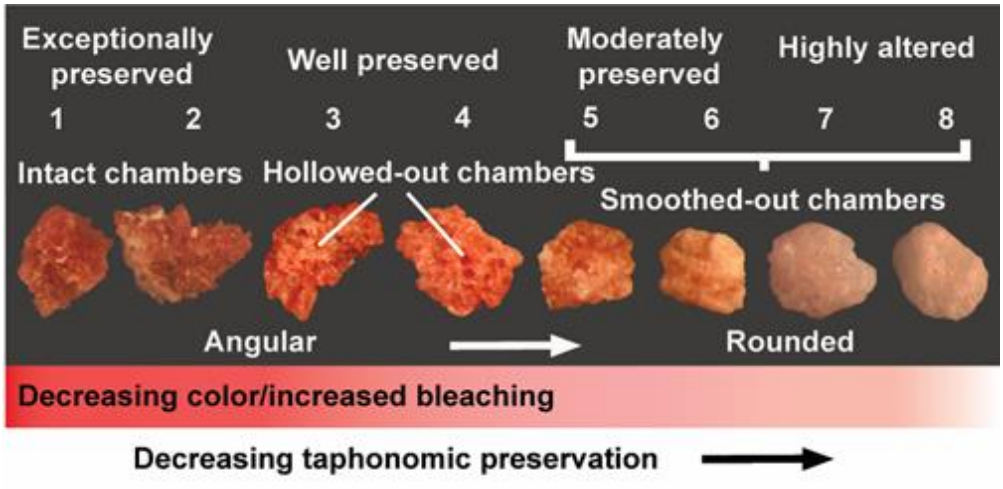

Figure 3: *Homotrema rubra*

Taphonomic states of *Homotrema rubra* according to Pilarczyk and Reinhardt (2012) listed in order of decreasing preservation. Exceptionally preserved individuals with red coloring, angular fragments, and intact chambers (1 - 2). Well-preserved individuals with pink coloring, angular fragments, and hollowed out chambers (3 – 4). Moderately preserved individuals with light pink coloring, slightly rounded fragments, and smoothed out chambers (5 – 6). Highly altered individuals with very light pink to white coloring, rounded edges, and smoothed-out chambers (7 – 8).

3.3 PAM cluster analysis

Partitioning Around Medoids (PAM) cluster analysis was used to document *Homotrema* distributions along transects WB, SP, and SS for each sampled time period (March 2017 to March 2019) according to the methods of Kemp et al. (2012). PAM cluster analysis was chosen due to its objective clustering algorithm; unlike other common clustering techniques, PAM cluster analysis is not user-biased because it objectively fits samples into a user-defined number of groups (Kaufman and Rousseeuw, 2009) and produces silhouette widths, which are a measure of the appropriateness of an individual sample's classification. The classification scale ranges from -1 to 1, where 1 represents a perfect fit into a group or cluster, while -1 is a perfectly incorrect fit. The

average silhouette width and percent accuracy (ecological appropriateness: percentage of samples clustered in the appropriate subenvironment) for a set of clustered data assists in determining which scenario is most appropriate (Kosciuch et al., 2018; Pilarczyk et al., 2020).

Prior to cluster analysis, the dataset was standardized by calculating z-scores for each sample. Z-scores are a means of standardizing a dataset by determining how many standard deviations a value is from the mean (Kaufman and Rousseeuw, 2009). Z-scores were then imported into the PAM 'cluster' package in R (e.g., Kaufman and Rousseeuw, 1990; Maechler et al., 2005).

Seven different data combinations (Tests 1 – 7: all possible combinations of concentration, taphonomy, and fragment size data) and five clustering scenarios (Tests 1 – 5: two to six cluster scenarios) were applied to each of the samples collected between March 2017 and March 2019 (Figs. S4-S6; Table S2). In transects WB and SP, where certain sampling intervals (e.g., March 2017 and August 2018) extended further offshore, only the stations represented in all three of the sampling intervals were used in cluster analysis (i.e., stations WB1 to WB15 were used; SP1 to SP15; SS1 to SS23).

The data combinations tested on each sample include: test 1 (*Homotrema* taphonomy), test 2 (concentration of *Homotrema* fragments), test 3 (size of *Homotrema* fragments), test 4 (taphonomy + concentration), test 5 (taphonomy + size), test 6 (concentration + size), and test 7 (taphonomy + concentration + size). These seven combinations were utilized in order to determine which data combination yielded the strongest clustering results (e.g. Figs. S4-S6; Table S2). Once an appropriate data combination was determined, PAM cluster analysis was used to test various scenarios

ranging from 2 to 6 clusters on each of the 182 samples shared between transects and used in cluster analysis (Table S2). The number of clusters was capped at 6 because clusters beyond that yielded plots with very low silhouette widths that did not make ecological sense. Using the most appropriate combination of data (test 4: taphonomy + concentration) and cluster scenario (3 clusters), plots for each transect were generated and the average silhouette width and associated percent accuracy calculated.

4. RESULTS

4.1 Windlass Bight (Transects WBa, WBb, WBc)

The Windlass Bight transect is approximately 650 m in length and is characterized by the following sub-environments: beach, reef flat, and reef crest (Fig. 4a). Water depths along the transect ranged between 0.3 and -1.1 m above sea level in 2017, 1.0 and -2.2 m in January 2018, and 1.0 and -1.4 m in August 2018.

PAM cluster analysis on samples collected in March 2017 (6 months before Hurricane Irma) revealed three groups corresponding to distance offshore: WB1.1 (-9 ± 9 m from the shoreline), WB1.2 (206 ± 150 m from the shoreline), and WB1.3 (519 ± 103 m from the shoreline) (Fig. 7). The groupings were characterized by an average silhouette width of 0.32 and 89% of samples clustered in ecologically appropriate groups. The first cluster (WB1.1) is characterized by supratidal samples collected from the beach and dune (average -9 m from shoreline). In general, samples in WB1.1 (Fig. 7) are dominated by low concentrations of *Homotrema* fragments (532 fragments per cm^3; Fig. 5), high abundances of highly altered fragments (46%), and large relative abundances (62%) of fragments in the medium size range (Fig. S1). In contrast, cluster WB1.2 (Fig. 7) consists exclusively of reef flat samples (average 206 m from shoreline) and is dominated by moderate concentrations of *Homotrema* (575 fragments per cm^3) that are predominantly exceptionally and well-preserved (46% combined), and mostly in the medium size range (53%). Similarly, cluster WB1.3 (Fig. 7) (average 519 m from shoreline) contains reef flat and some reef crest samples. This cluster is characterized by high concentrations of *Homotrema* fragments (631 fragments per cm^3), high relative abundances of

exceptionally preserved and well-preserved fragments (57% combined), and a predominance of fragments in the medium size range (57%).

In general, concentrations of *Homotrema* collected in January 2018 (WBb; 4 months after Irma) were slightly higher than those from 2017 (696 per cm^3 in 2018 vs 587 per cm^3 in 2017) and had higher abundances of exceptionally preserved and well-preserved fragments (56% combined in 2018 vs 46% combined in 2017) with test sizes that were predominantly in the medium size fraction (Fig. 4). In general, the WBb transect (with average samples distances of WB2.1: 89 ± 79 WB2.2: -6 ± 0 WB2.3: 376 ± 187 m from shoreline) is characterized by high concentrations of *Homotrema* (696 per cm^3) that showed a lack of clear zonation (i.e., homogenization) between the beach, reef flat, and reef crest environments (average silhouette width = 0.39; accuracy = 47%). This is in contrast to WBa, which had a high accuracy value (89%). Cluster WB2.1 (89 m from shoreline), which contains both beach and reef flat samples, is dominated by high concentrations of *Homotrema* fragments (715 fragments per cm^3), high abundances of exceptionally and well-preserved fragments (48%), as well as abundances (65%) of fragments in the medium size fraction. Cluster WB2.2 (-6 m from shoreline), which consists solely of one beach sample, is characterized by a low concentration of *Homotrema* fragments (365 fragments per cm^3), high relative abundance of highly altered fragments (41% combined), and a large relative abundance (74%) of fragments that are medium in size. Cluster WB2.3 (376 m from shoreline), contains samples from the reef crest and reef flat, has the highest concentrations of *Homotrema* fragments (757 fragments per cm^3), as well as high relative abundances of exceptionally preserved and

well-preserved fragments (74% combined), and a high relative abundance (67%) of fragments that are medium in size.

Overall, *Homotrema* concentrations from WBc (August 2018) were lower than in WBb (January 2018) (602 per cm^3 in August 2018 vs 696 per cm^3 in January 2018) and have lower abundances of exceptionally preserved and well-preserved fragments (43% combined in August 2018 vs 55% combined in January 2018). In August 2018 (11 months after Irma), WBc was characterized (with average sample distances of WB2.1: -5 ± 10 WB2.2: 154 ± 63 WB 2.3: 454 ± 106 m from shoreline) by moderate concentrations of *Homotrema* (602 per cm^3) that showed a distinction between samples collected from the beach, reef flat, and reef crest environments (average silhouette width = 0.58; accuracy = 80%), which was similar to cluster WBa, which showed similar silhouette width and accuracy values (e.g., 0.32 and 89% respectively). The first cluster (WB3.1; -5 m from shoreline) includes two beach samples and one reef flat sample near the shore and is dominated by low concentrations of *Homotrema* fragments (526 fragments per cm^3), high abundances of highly altered fragments (51%), and a large relative abundance (50%) of fragments that were medium in size. The second cluster (WB3.2, 154 m from shoreline) includes reef flat samples and is dominated by a moderate concentration of *Homotrema* fragments (558 fragments per cm^3), moderate abundances of exceptionally and well-preserved fragments (38%), and a high relative abundance (51%) of fragments that were medium in size. The third cluster (WB3.3, 454 m from shoreline) is dominated by a high concentration of *Homotrema* fragments (626 fragments per cm^3), high relative abundances of exceptionally preserved and well-preserved fragments (60% combined), and a large relative abundance (48%) of fragments that were medium in size.

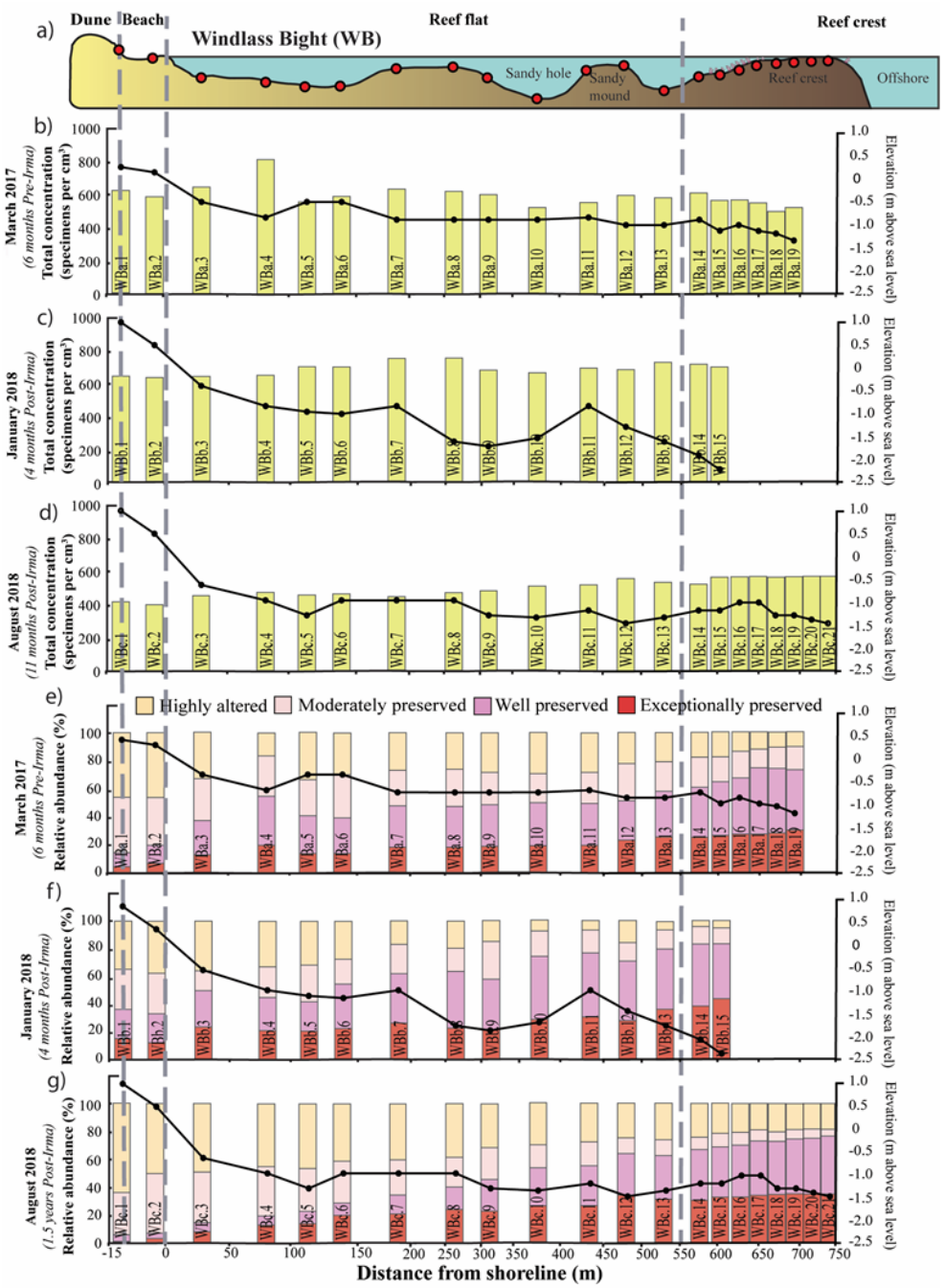

Figure 4: *Windlass Bight concentration and taphonomy*

Homotrema distributions along the Windlass Bight (WB) transect (north side of Anegada) relative to increasing distance offshore. (a) Nearshore cross-section of WB indicating sample locations (red circles) and major geomorphic changes along transect. Total concentration of *Homotrema* individuals per 1 cm^3 (b – d) and relative abundances (%) of each taphonomic category (e – g) in each of the three sampling intervals. Corresponding surface elevation profiles indicated by a solid black line. Vertical dashed lines represent a change from one subenvironment to the next (e.g. beach to reef flat).

4.2 Soldier Point (Transects SPa, SPb, SPc)

The Soldier Point transect is approximately 150 m in length and is characterized by the following sub-environments: beach, reef flat, and reef crest (Fig. 5a). Water depths along the transect ranged between 1.0 and -1.0 m above sea level in 2017, 1.0 and -1.3 m in January 2018, and 1.0 and -1.3 m in March 2019.

PAM cluster analysis conducted on samples collected in March 2017 (6 months before Hurricane Irma) revealed three groups corresponding to distance offshore: SP1.1 (24 ± 27 m), SP1.2 (88 ± 19 m), and SP1.3 (138 ± 14 m) (Fig. 7). The groupings were characterized by an average silhouette width of 0.43 and 89% of samples clustered in ecologically appropriate groups. The first cluster (SP1.1) is characterized by supratidal samples collected from the beach and dune (average 24 m from shoreline). In general, samples in SP1.1 (Fig. 7) are dominated by low concentrations of *Homotrema* fragments (514 fragments per cm^3; Fig. 5), high abundances of highly altered fragments (56%), and large relative abundances (47%) of fragments medium in size range (Fig. S2). In contrast, cluster SP1.2 (Fig. 7) consists exclusively of reef flat samples (average 88 m from shoreline) and is dominated by moderate concentrations of *Homotrema* (614 fragments per cm^3) that are predominantly exceptionally and well-preserved (48% combined), and mostly in the medium size range (56%). Similarly, cluster SP1.3 (Fig. 7; average 138 m from shoreline) contains reef flat and some reef crest samples. This cluster is characterized by high concentrations of *Homotrema* fragments (693 fragments per cm^3), high relative abundances of exceptionally preserved and well-preserved fragments (64% combined), and a predominance of fragments in the medium size range (52%).

In general, concentrations of *Homotrema* collected in January 2018 (SPb; 4 months after Irma) were slightly higher than those from 2017 (696 per cm^3 in 2018 vs 587 per cm^3 in 2017) and had higher average abundances of exceptionally preserved and well-preserved fragments (56% combined in 2018 vs 46% combined in 2017) with test sizes that were predominantly in the medium size fraction (Fig. 5). In general, the SPb transect (average sample cluster distances SP2.1: 14 ± 20; SP2.2: 84 ± 13; SP2.3: 121 ± 21 m from shoreline) is characterized by high concentrations of *Homotrema* (696 per cm^3) that showed a lack of clear zonation (i.e., homogenization) between the beach, reef flat, and reef crest environments (average silhouette width = 0.45; accuracy = 67%). This is in contrast to SPa which had a high percent accuracy compared to SPb (89%), and showed clear zonation between these environments. Cluster SP2.1 (Fig. 7; 14 m from shoreline), which contains both beach and reef flat samples is dominated by high concentrations of *Homotrema* fragments (612 fragments per cm^3), high abundances of exceptionally and well-preserved fragments (50%), as well as abundances (49%) of fragments in the medium in size fraction. Cluster SP2.2 (Fig 7; 84 m from shoreline), which consists solely of one beach sample, is characterized by a low concentration of *Homotrema* fragments (721 fragments per cm^3), high relative abundances of highly altered fragments (72% combined), and large relative abundances (47%) of fragments in the medium size range. Cluster SP2.3 (Fig. 7; 121 m from shoreline), contains samples from the reef crest and reef flat, has the highest concentrations of *Homotrema* fragments (858 fragments per cm^3), as well as high relative abundances of exceptionally preserved and well-preserved fragments (83% combined), and large relative abundances (40%) of fragments in the medium size range.

Overall, *Homotrema* concentrations from SPc (March 2019) were lower than in SPb (January 2018) (541 per cm^3 in March 2019 vs 696 per cm^3 in January 2018) and have lower abundances of exceptionally preserved and well-preserved fragments (38% combined in March 2019 vs 59% combined in January 2018). In March 2019 (18 months after Irma), SPc was characterized (average sample cluster distances SP3.1: 12 ± 21; SP3.2: 79 ± 18; SP 3.3: 125 ± 9 m from shoreline) by moderate concentrations of *Homotrema* (541 per cm^3) that showed zonation between the beach, reef flat, and reef crest environments (average silhouette width = 0.54; accuracy = 80%), which was similar to cluster SPa, which showed similar silhouette widths and accuracy values (0.43 and 89%). The first cluster (SP3.1, 12 m from shoreline) includes two beach samples and one reef flat sample near the shore and is dominated by low concentrations of *Homotrema* fragments (473 fragments per cm^3), high abundances of highly altered fragments (66%), and a large relative abundance (61%) of fragments that were medium in size. The second cluster (SP3.2, 79 m from shoreline) includes reef flat samples and is dominated by a moderate concentration of *Homotrema* fragments (544 fragments per cm^3), moderate abundances of exceptionally and well-preserved fragments (44%), and high relative abundances (55%) of fragments that were medium in size. The third cluster (SP3.3, 125 m from shoreline) is dominated by a high concentration of *Homotrema* fragments (640 fragments per cm^3), high relative abundances of exceptionally preserved and well-preserved fragments (59% combined), and large relative abundances (52%) of fragments that were medium in size.

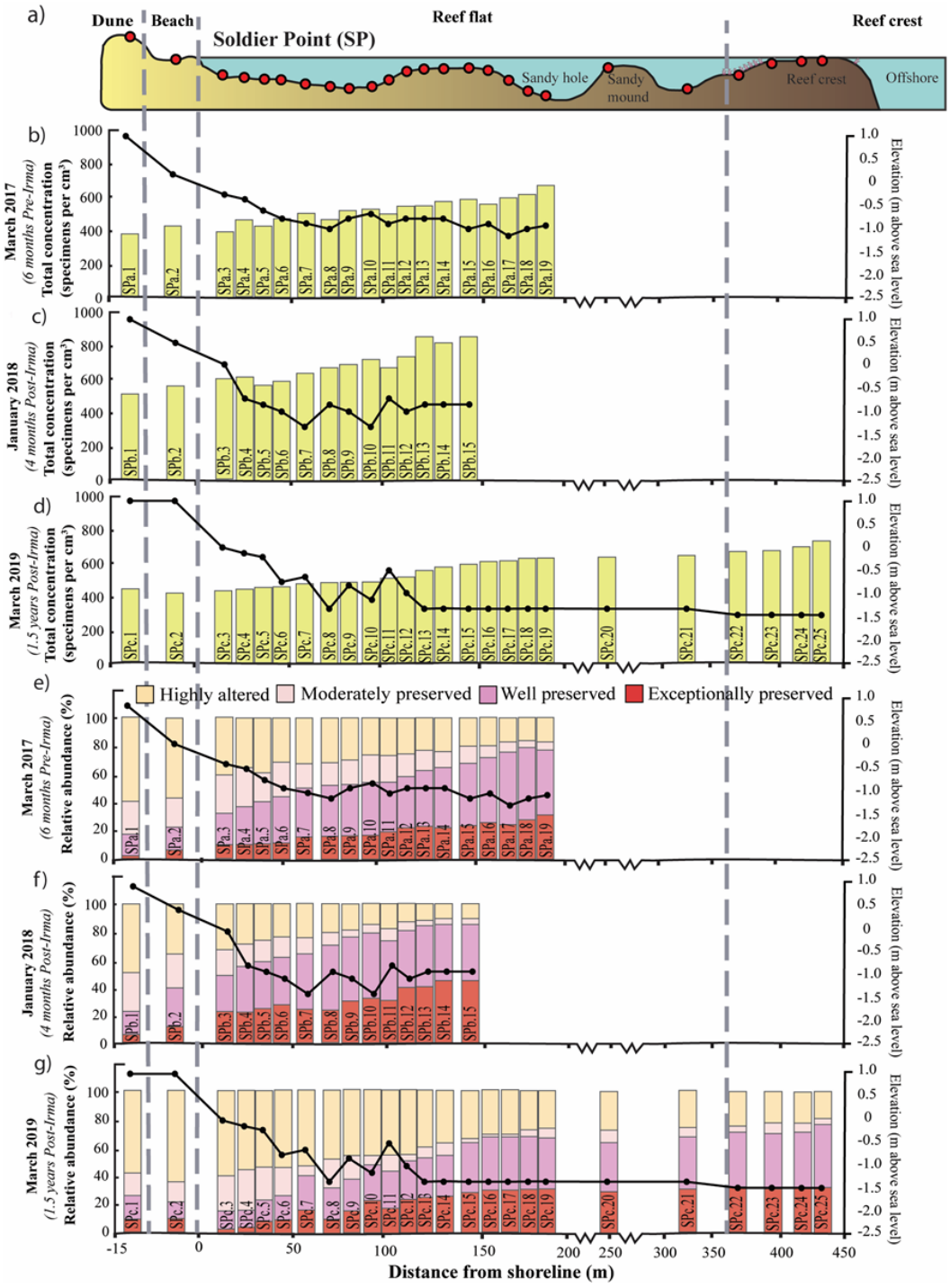

Figure 5: *Soldier Point concentration and taphonomy*

Homotrema distributions along the Soldier Point (SP) transect (north side of Anegada) relative to increasing distance offshore. (a) Nearshore cross-section of SP indicating sample locations (red circles) and major geomorphic changes along transect. Total concentration of *Homotrema* individuals per 1 cm^3 (b – d) and relative abundances (%) of each taphonomic category (e – g) in each of the three sampling intervals. Corresponding surface elevation profiles indicated by a solid black line.

4.3 South of Settlement (Transects SSa, SSb, SSc)

The South of Settlement (SS) transect is approximately 1380 m in length and is characterized by: beach, mud flat, and coral mound subenvironments (Fig. 6a). Water depths along the transect ranged between 0.4 and -1.0 m above sea level in 2017, 1.0 and -1.7 m in January 2018, 0.1 and -1.5 m in August 2018, and 0.1 and -1.2 m in March 2019.

PAM cluster analysis on samples collected in March 2017 (6 months before Hurricane Irma) revealed three groups corresponding to distance offshore: SS1.1 (-5 ± 7 m), SS1.2 (844 ± 347 m), and SS1.3 (1254 ± 9 m) (Fig. 7). The groupings were characterized by an average silhouette width of 0.57 and 95% of samples clustered in ecologically appropriate groups. The first cluster (SS1.1) is characterized by beach samples (average -5 m from shoreline). In general, samples in SS1.1 (Fig. 7) are dominated by low concentrations of *Homotrema* fragments (378 fragments per cm^3; Fig. 6), high abundances of highly altered fragments (72%), and high relative abundances (47%) of fragments in the medium size range (Fig. S1). In contrast, cluster SS1.2 (Fig. 7) consists of mud flat and coral mound samples (average 844 m from shoreline) and is dominated by low concentrations of *Homotrema* (435 fragments per cm^3) that are predominantly highly altered (56%), and mostly in the medium size range (42%). Similarly, cluster SS1.3 (average 1254 m from shoreline) contains mud flat and coral mound samples. This cluster is characterized by low concentrations of *Homotrema* fragments (325 fragments per cm^3), high relative abundances of highly altered fragments (56%), and a predominance of fragments in the medium size range (44%).

In general, concentrations of *Homotrema* collected in January 2018 (SSb; 4 months after Irma) were higher than those from 2017 (680 per cm^3 in 2018 vs 415 per cm^3 in 2017) and had higher abundances of exceptionally preserved and well-preserved fragments (9% combined in 2018 vs 3% combined in 2017) with test sizes that were predominantly in the medium size fraction (Fig. 6). In general, the SSb transect (with average samples distances of SS2.1: 876 ± 594 SS2.2: 653 ± 360 SS2.3: 1209 ± 119 m from shoreline) is characterized by high concentrations of *Homotrema* (680 per cm^3) that showed a lack of clear zonation (i.e., homogenization) between the beach, reef flat, and reef crest environments (average silhouette width = 0.4; accuracy = 65%). This is in contrast to SSa, which had a higher silhouette width and accuracy value (0.57; 95%). Cluster SS2.1 (876 m from shoreline), which contains both beach and mud flat samples, is dominated by moderate concentrations of *Homotrema* fragments (578 fragments per cm^3), high abundances of highly altered fragments (57%), as well as high abundances (48%) of fragments in the medium in size fraction. Cluster SS2.2 (653 m from shoreline), which consists of beach, mud flat, and coral mound samples, is characterized by a high concentration of *Homotrema* fragments (704 fragments per cm^3), high relative abundance of highly altered fragments (53% combined), and a large relative abundance (51%) of fragments medium in size. Cluster SS2.3 (1209 m from shoreline), contains samples from the mud flat and coral mounds, has the highest concentrations of *Homotrema* fragments (816 fragments per cm^3), as well as high relative abundances of highly altered fragments (45% combined), and a large relative abundance (49%) of fragments medium in size. Overall, *Homotrema* concentrations from SSc (August 2018) were lower than in SSb (January 2018) (422 per cm^3 in August 2018 vs 680 per cm^3 in January 2018) and have

lower abundances of exceptionally preserved and well-preserved fragments (3% combined in August 2018 vs 9% combined in January 2018). In August 2018 (11 months after Irma), SS1.3 was characterized (with average samples distances of SS2.1: -3 ± 4 SS2.2: 876 ± 377 SS 2.3: 888 ± 320 m from shoreline) by moderate concentrations of *Homotrema* (422 per cm^3) that lacked zonation between the beach, reef flat, and reef crest environments (average silhouette width = 0.28; accuracy = 70%). The first cluster (SS3.1, -3 m from shoreline) includes beach samples and is dominated by low concentrations of *Homotrema* fragments (490 fragments per cm^3), high abundances of highly altered fragments (71%), and a large relative abundance (46%) of fragments that were medium in size. The second cluster (SS3.2, 876 m from shoreline) includes mud flat and coral mound samples and is dominated by a low concentration of *Homotrema* fragments (499 fragments per cm^3), high abundances of highly altered fragments (56%), and a large relative abundance (52%) of fragments medium in size. The third cluster (SS3.3, 888 m from shoreline) consists of mud flat and coral mound samples and is dominated by a low concentration of *Homotrema* fragments (379 fragments per cm^3), high relative abundance of highly altered fragments (57% combined), and a large relative abundance (47%) of fragments that were medium in size.

In general, *Homotrema* concentrations from SSd (March 2019) were higher than in SSc (August 2018) (447 per cm^3 in March 2019 vs 422 per cm^3 in August 2018) and had near identical abundances of exceptionally preserved and well-preserved fragments (3% combined in March 2019 vs 3% combined in August 2018). In March 2019 (11 months after Irma), SSd was characterized (with average samples distances of SS2.1: 769 ± 491 SS2.2: 634 ± 404 SS2.3: 860 ± 187 m from shoreline) by moderate concentrations

of *Homotrema* (447 per cm^3) that lacked obvious zonation between the beach, mud flat, and coral mound environments (average silhouette width = 0.44; accuracy = 70%), but did distinctly separate the coral mound samples into their own cluster (cluster SS3.3). The first cluster (SS3.1, 769 m from shoreline) includes one coral mound sample along with beach and mud flat samples and is dominated by low concentrations of *Homotrema* fragments (425 fragments per cm^3), high abundances of highly altered fragments (85%), and large relative abundances (53%) of fragments that were medium in size. The second cluster (SS3.2, 634 m from shoreline) includes mud flat and coral mound samples and is dominated by a low concentrations of *Homotrema* fragments (453 fragments per cm^3), moderate abundances of highly altered fragments (78%), and high relative abundances (55%) of fragments that were medium in size. The third cluster (SS3.3, 860 m from shoreline) consists entirely of coral mound samples and is dominated by a low concentration of *Homotrema* fragments (484 fragments per cm^3), high relative abundance of highly altered fragments (68% combined), and a large relative abundance (45%) of fragments that were medium in size.

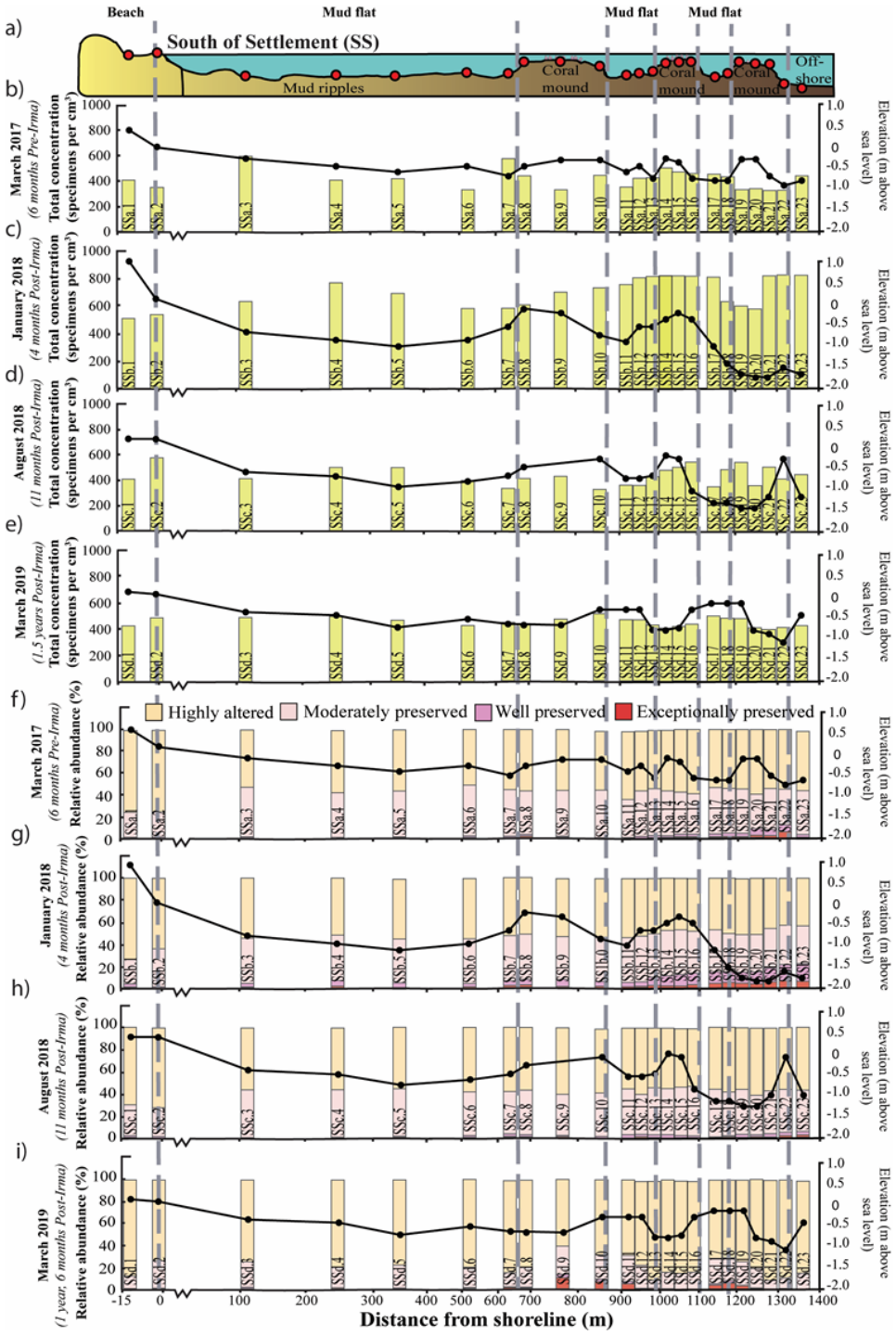

Figure 6: *South of Settlement concentration and taphonomy*

Homotrema distributions along the South of Settlement (SS) transect (south side of Anegada) relative to increasing distance offshore. (a) Nearshore cross-section of SS indicating sample locations (red circles) and major geomorphic changes along transect. Total concentration of *Homotrema* individuals per 1 cm^3 (b – e) and relative abundances (%) of each taphonomic category (f – i) in each of the four sampling intervals. Corresponding surface elevation profiles indicated by a solid black line.

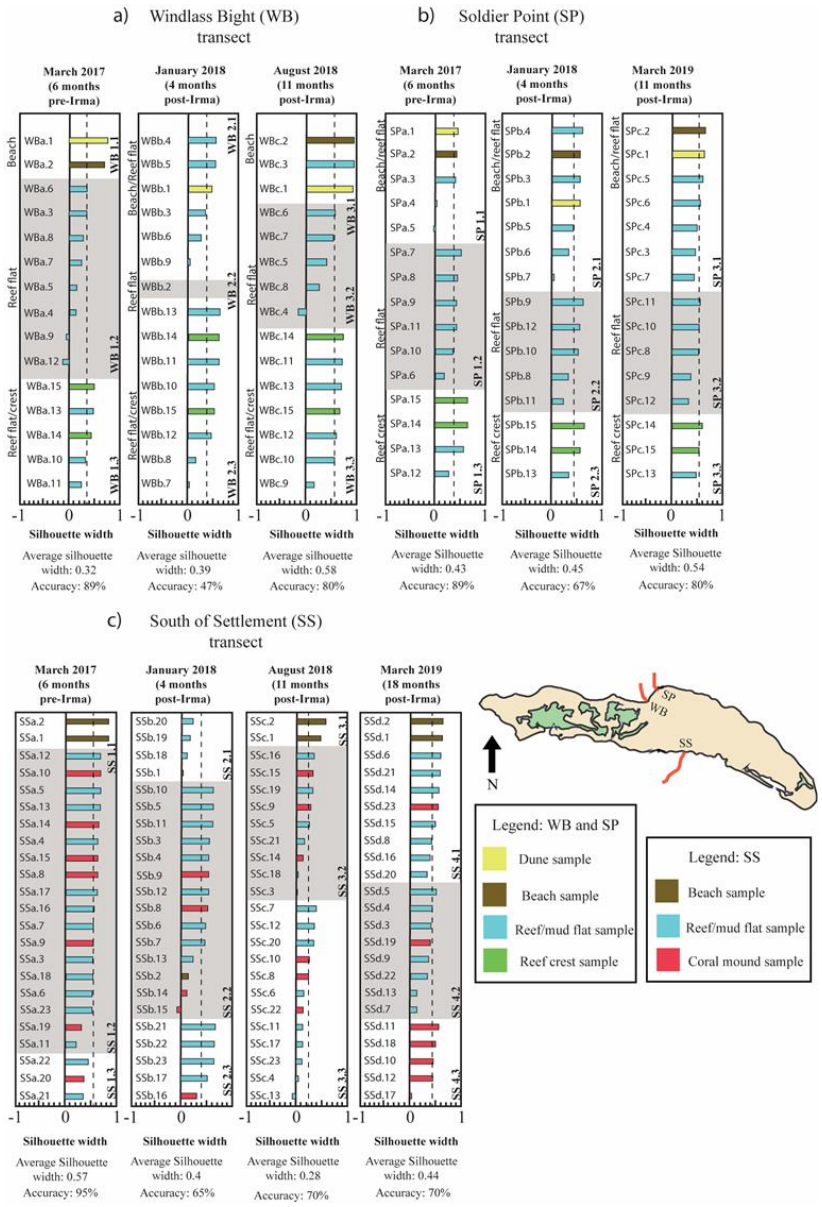

Figure 7: *PAM cluster analysis*

Results of PAM cluster analysis for WB (a), SP (b), and SS (c) transects showing changes within the *Homotrema* distributions before and after Hurricane Irma. The northern transects (WB and SP) have coverage of a fringing reef and are reflective of a more energetic wave regime while the southern transect (SS) has no reef coverage and is much lower wave energy with mud flats and coral mounds instead of the typical reef transect environment. For each scenario, the average silhouette width (indicated by dashed line) and the percent accuracy (i.e., percentage of samples that clustered in the appropriate environment) are indicated. Clusters are represented by either a white space (e.g. WB 1.1 and 1.3) or a grey box (WB1.2). Samples within a cluster represent similar taphonomic characteristics and *Homotrema* concentrations, while the percent accuracy is a reflection of how well samples within a cluster grouped based on their ecological niche.

5. DISCUSSION

5.1 *Homotrema* as a sediment transport indicator

Homotrema lives attached to coral reefs and other hard substrates and predictably bleaches from red to white as a result of ultraviolet light exposure following detachment from its substrate (MacKenzie et al., 1965). In this respect, *Homotrema*-bearing sediments have a defined provenance, making the foraminifer a useful sediment transport indicator (Machado and Moraes, 2002; Pilarczyk and Reinhardt, 2012; Pilarczyk et al., 2014b). With increased residence time, the shape of a *Homotrema* fragment becomes progressively more rounded and bleached (Pilarczyk et al., 2014b). This change in physical condition of the test, or taphonomy, results in a predictable pattern with increasing distance from the reef sourced that was first described by MacKenzie et al. (1965).

The predictability with which *Homotrema* becomes taphonomically altered following detachment from the reef has been documented along several coral reef coastlines including the British Virgin Islands, Bermuda, Polynesia, Brazil, and Indonesia (Machado and Moraes, 2002; Pilarczyk et al., 2012; Pilarczyk et al., 2014b; Alam et al., 2018). Distributions of *Homotrema* along Anegada's northern shore (Transects WBa,b,c and SPa,b,c) show a similar trend where dune/beach, reef flat, and reef crest samples are distinct from one another based on color, angularity, and chamber preservation. For example, dune and beach sediments contain *Homotrema* that are highly altered or moderately preserved; whereas, reef crest sediments, those closest to the source of *Homotrema*, are characterized by exceptionally or well-preserved fragments (Fig. 4; Fig. 5). PAM cluster analysis on the pre-Hurricane Irma data (i.e., WBa and SPa) corroborate

this trend by showing three distinct groupings corresponding to beach, reef flat, and reef crest environments (Fig. 7). This is similar to *Homotrema* distributions reported in Polynesia, where *Homotrema* taphonomy was able to distinguish between outer reef, reef crest, reef apron, lagoon, and island sub-environments (Pilarczyk et al., 2014b). This was also the case in Brazil, where *Homotrema* taphonomy was able to differentiate between the back reef, fore reef, and shallow reef flat zones (Machado and Moraes 2002); in Mexico, where coral reef foraminiferal assemblages, which included *Homotrema rubra*, were able to distinguish between the windward margin, the western platform interior, eastern platform interior, and the leeward margin patch reef (Gischler and Moder 2009); Bermuda; and in French Polynesia, where coral reef assemblages were able to distinguish between peripheral and central lagoon areas associated with an atoll (Bichi et al., 2002). In this way, *Homotrema* can be used to identify sub-environments within a reef setting, and therefore, constrain provenance of transported sediment. This becomes particularly useful when identifying overwash deposits in reef environments. Owing to the erosive nature and high transport capacity of tsunami and storm waves, overwash deposits in locations such as Anegada are recognized by layers of red to pink sand (Atwater et al., 2012; Pilarczyk and Reinhardt, 2012) that often contain exceptionally to well-preserved *Homotrema* fragments in high concentrations (Atwater et al., 2012; Pilarczyk and Reinhardt, 2012).

5.2 Variability within *Homotrema* distributions

Homotrema distributions along the two northern transects (WB and SP), spaced 525 m apart, did not vary significantly. At Windlass Bight, the WBa transect (6 months before Hurricane Irma) separated beach/dune samples (WB1.1) from reef flat (WB1.2)

and reef crest (WB1.3) samples with an average silhouette width of 0.32 and an accuracy value of 89%. The groupings were largely correlated and explained by distance from the shoreline, with WB1.1 consisting of samples within -9 m of the shoreline, WB1.2 within 206 m, and WB1.3 within 519 m. A similar trend was noticed at Soldier Point, where the same three groupings produced and average silhouette width of 0.43 and 89% of samples clustered in the subenvironment from which they were collected (Fig. 7). In general, the groupings obtained from cluster analysis were largely attributed to distance from the shoreline. For example, SP1.1 consisted of samples within 24 m of the shoreline, SP1.2 within 88 m, and SP1.3 within 138 m. Similarly, WB1.1 consisted of samples within -9 m of the shoreline, WB1.2 within 206 m, and WB1.3 within 519 m.

While both northern transects showed similar distributions of *Homotrema*, Soldier Point samples, in general, had greater relative abundances of well-preserved specimens than Windlass Bight. For example, Soldier Point samples had on average 4% more exceptionally- to well-preserved fragments over all transects when compared to Windlass Bight samples. This discrepancy can be attributed to the fact SP is situated closer to the fringing reef, and therefore, the source of *Homotrema* (Phalen et al., 2016) and because Soldier Point's wave regime is also more energetic.

Although distributions along the northern transects were relatively consistent in terms of concentration, degree of preservation, and test size, they varied significantly when compared to the SS transect established on the southern side of Anegada. In general, concentrations of *Homotrema* were significantly less on the southern side of the island relative to the northern side. For example, concentrations of the reef flat samples in WBa ranged from 517 to 816 fragments per cm^3; where as they ranged from 320 to 606

fragments per cm^3 at SSa (Fig. 7). *Homotrema* distributions along the SSa transect were predominantly highly altered (51-76%), with very few that were exceptionally preserved (0-10%). This was noted previously by Pilarczyk and Reinhardt (2012) who speculated that the patch reefs to the south of Anegada would not produce as many individuals as the northern fringing reefs due to their lack of coverage and declining health, resulting in lower concentrations of *Homotrema*. The low concentrations of *Homotrema* observed at SS are likely sourced from a combination of patch reefs and transported sediments from the western and eastern sides of the island (Figure 1). In addition, Irma had lesser of an impact on the southern shore of the island due to a smaller storm surge (Spiske et al., in progress).

In addition to lower concentrations of *Homotrema* on the southern side of Anegada, it was observed that of the fragments present, most were highly altered (51-76%). The lack of well-preserved *Homotrema* at SS could be due to differing wave climates between the south and north, similar to what was observed in Polynesia (Pilarczyk et al., 2014b). Wave climates to the north would be significantly different due to the increased wave energy during both baseline and storm conditions as opposed to the more sheltered and low-energy southern side of the island, where for hundreds of meters the water depth ranges from 0.3 to 0.5 m and the water is relatively calm. Higher wave energy would assist in detaching more *Homotrema*, thereby increasing the concentration of fragments in nearby sediments. Similarly, Machado and Moraes (2002) found that *Homotrema* obtained from the Praia de Forte reef system, which has high energy waves were found to be red and angular; whereas the lower energy Rio do Fogo reefs contained more bleached and rounded specimens.

5.3 Impact of storms on modern surface distributions of *Homotrema*

Modern distributions of microfossil assemblages are used to determine provenance for overwash deposits because they serve as a baseline for comparison with the paleorecord (Horton et al., 2009; Hippensteel and Martin 2014; Nishijama et al., 2015; Kosciuch et al., 2018; Soria et al., 2018). Modern distributions can be used to identify specific point sources of sediment available for transport by overwash events (Kosciuch et al., 2018; Pilarczyk et al., 2019), which assists in understanding sediment provenance and distance of sediment transport. Several studies have documented modern foraminiferal distributions (Kosciuch et al., 2018; Pilarczyk et al., 2020), using a combination of taxonomic and taphonomic data, yet it remains unclear the degree to which large storms and tsunamis impact the distributions and concentrations of the microfossil assemblage.

Hurricane Irma inundated several parts of Anegada, resulting in storm surge flow depths up to 3.8 meters above sea level on the north side of the island and less than 2 meters above sea level on the south side (Spiske et al., in prep) as well as overwash fans that extended tens of meters inland. As a result of this overwash event, the nearshore surface sediments at Anegada, particularly on the northern side of the island, were homogenized. Hurricane Irma altered the nearshore sediment assemblages by increasing the concentration of the *Homotrema* fragments along the transects and homogenizing the sediment. This resulted in clusters with a greater number of samples that were grouped incorrectly (WB accuracy lowered from 89% in 2017 to 47% in January 2018; SP accuracy lowered from 89% in 2017 to 67% in January 2018; SS accuracy lowered from 95% in 2017 to 65% in January 2018). This homogenizing effect as a result of Hurricane

Irma's storm surge, is consistent with findings from Australia after Cyclone Hamish (Strotz et al., 2016). At Anegada, the homogenizing effect returned to near pre-Hurricane Irma conditions within 1.5 years. This is in contrast to Heron Island coral reefs impacted by Cyclone Hamish, which took approximately six months longer (Strotz et al., 2016). At Anegada, an increase in the relative abundances of *Homotrema rubra* specimens resulted from Hurricane Irma's impact, but at Heron Island, the coral reef environment impacted by Hamish observed a decrease in relative abundance for many species of coral reef foraminifera (Strotz et al., 2016). These discrepancies highlight the need for site-specific modern distribution studies and show the variability within recalibration intervals associated with different environments and extreme wave events of varying intensity.

5.4 Recalibration of nearshore sediments after an overwash event

Following Hurricane Irma's storm surge and the subsequent homogenization of nearshore sediments at Anegada, the recalibration phase began as taphonomic assemblages and the total concentration of *Homotrema* fragments began to decrease and return back to pre-Irma conditions. In general, the concentration of *Homotrema* fragments recalibrated faster than the taphonomic and test size assemblages. After the initial increase in *Homotrema* concentration and preservation due to Hurricane Irma, the Soldier Point transect had notable decreases in both during the March 2019 field season, returning to pre-Irma levels. March 2017, before Irma, contained an average of 15 percent exceptionally preserved fragments, and after recovering from Irma in March 2019, sediments contained an average of 15 percent exceptionally preserved fragments. This showed that the environment had recalibrated in Soldier Point 1.5 years after Irma's landfall. The Windlass Bight transect was not sampled in March 2019 due to time

constraints, however, it still was able to return to levels that are similar to pre-Irma conditions despite less time to recover. Prior to Hurricane Irma, Windlass Bight sediments averaged 18% exceptionally preserved fragments, and in August 2018, nearly 12 months after Hurricane Irma, sediments averaged 22% exceptionally preserved fragments. What remains unclear however, is what caused the recovery time for the South of Settlement site to be longer than that seen in the northern transects. Factors that may influence the recovery of nearshore sediments include tidal range, the wave climate, the number and intensity of smaller storms, and the distance to the source of *Homotrema* in the reef. Surface sediments from South of Settlement experienced homogenization from Hurricane Irma's storm surge, and this homogenization was followed by two subsequent field seasons in August 2018 and March 2019 that showed zonations that were closer to pre-Irma conditions, but still did not indicate a full recovery (Fig. 7). Possible explanations for why this site did not recalibrate to pre-Hurricane Irma conditions within the time frame of the study include the lack of *Homotrema* fragments in the area and the lower wave-energy wave climates on the north side of the island.

Studies conducted in other settings have also reported on the impact that extreme wave events have on nearshore sediment assemblages. For example, Yannarell et al. (2007) investigated how microbial communities in a Bahamian salt pond responded to and recovered from Hurricane Frances' landfall. The study documented significant disturbance in the microbial community due to an influx of sand burying the microbial mat, but rapid recovery followed within approximately five weeks. Seike et al. (2013) examined benthic animal populations in the nearshore environment after the 2011 Tohoku-Oki tsunami and found that many populations began re-establishing within 1.5

years after the initial disturbance. This study reported that Otsuchi and Funakoshi bays were both disturbed by the tsunami by either a change in grain size from muddy to coarse sand, by an influx of sand from the tsunami (Otsuchi Bay), or by a change in bathymetry (Funakoshi Bay). The influxes of sand caused the removal of large burrows and fecal mounds which resulted in a more homogenized environment in some locations, and little to no change in grain size and bathymetry in other locations. The impact of some of these changes led to a destabilization of the megabenthos species such as clams, sea snail, and echinoids, and some of these species began re-establishing after the initial disturbance 18 months later. In general, the pattern of re-establishment of both grain size and megabenthos was rapid, indicating that recovery after 6 months is more substantial than prior to six months.

Another study examined how the disturbance of Cyclone Hamish led to a disturbance and subsequent recovery of tropical reef foraminifera, and this revealed that recovery took up to two years (Strotz et al., 2016). In this study, reef foraminifera assemblages became homogenized after a nearly direct impact from the cyclone, and resulted in a pronounced reduction in foraminiferal diversity. The recalibration of the assemblage back to pre-cyclone conditions was progressive, although recovery from 2010 to 2011 was slightly faster than the previous years. In regards to recalibration, similar results were found when analyzing microfossils contained within sediments off the coast of Thailand taken before and after the Indian Ocean tsunami (Sugawara et al., 2009). The tsunami disturbed the natural distribution of foraminiferal assemblages containing *Ammobaculites, Ammonia, Elphidum*, and *Rosalina*, and it was found that *Ammonia* and *Rosalina* species returned to their normal distribution patterns after two

years, although Elphidium and Ammobaculites did not fully return to their pre-event state (Sugawara et al., 2009). This was likely due to tsunami backwash transporting foraminiferal species to deeper areas (Sugawara et al., 2009). Our study, also conducted in a carbonate reef environment with a similar hurricane intensity like the conditions of Cyclone Hamish impacting Heron Island, similarly found that the nearshore sediments returned to near pre-Irma levels of taphonomy and concentration in the north around 1.5 years.

Based on our results from Anegada, it is recommended that future work in reef-dominated environments similar to Anegada wait at least a year and a half after a major disturbance to sample the nearshore environment to ensure that the samples are representative of the baseline distributions of assemblages in various subenvironments. With that in mind, it should be noted that the results in this study are representative of a Category 5 storm that did not make a direct impact on the island, which would likely impact recovery time. This assumption is supported by the results from Cyclone Hamish (Strotz et al., 2016), which showed similar intensity (Category 4) also in a carbonate reef environment. The Heron Island reef underwent a higher degree of change to its microfossil assemblage than observed in Anegada, resulting in a longer recovery interval, likely because of the more direct strike Cyclone Hamish had on the site. Tropical cyclones with higher storm surges may result in greater homogenizations, and therefore, longer recalibration intervals. Areas that experience frequent overwash inundation (multiple storms a year) may need to reconsider what is considered baseline conditions for the site before applying modern distribution methods for overwash comparison.

6. CONCLUSION

Distributions of *Homotrema rubra* are useful sediment transport indicators in reef settings as they aid in constraining the provenance of transported sediment. *Homotrema*'s utility as a sediment transport indicator is enhanced when in the presence of a direct source (i.e., reef). At Anegada, distributions of *Homotrema* showed a clear relationship with distance from the reef; however, along Anegada's southern shores, where there is no expansive fringing reef, *Homotrema* distributions were less concentrated, more homogenized, and likely transported from the western and eastern sides of the island. The degree to which these southern distributions recover after being altered by large overwash events (i.e., hurricanes, tsunamis) remains unclear.

Hurricane Irma's landfall in September 2017, an extreme, but short-lived, disturbance on the nearshore surface sediments of Anegada, BVIs resulted in a 12-16% overall increase in the concentration of *Homotrema* in the north, where most of the fragments were exceptionally and well preserved. PAM cluster analysis revealed a homogenizing effect attributed to Hurricane Irma, where the percentage of samples that clustered in the appropriate environment decreased from 89% to 47% to 80% over a time period of 7 months at Windlass Bight and from 89% to 67% to 80% over a period of 18 months at Soldier Point. The sediments remained homogenized, without a clear relationship with distance from the reef source until August 2018 in WB and March 2019 in SP, where concentrations and the taphonomic condition of samples along the transects returned to near pre-Hurricane Irma conditions. In general, *Homotrema* distributions did not return to pre-Hurricane Irma conditions until 1.5 years after the storm impacted the Anegada coastline. This recalibration interval is consistent with other locations, including Japan,

where sediments disturbed by the 2011 Tohoku tsunami required 1.5 years to return to pre-tsunami conditions.

It is important to note that recalibration intervals may be site and event specific. As a result, future studies employing surface distributions of sediments as a basis of comparison with paleo-overwash deposits need to ensure that sufficient time has elapsed between collection and the most recent extreme perturbations. For the BVIs, this interval appears to be approximately 1.5 years for a Category 5 hurricane that did not make direct landfall on the study area. Larger or smaller hurricanes with direct or indirect impacts on a tropical island may result in different recalibration times.

APPENDIX A

Table S1: *Homotrema Data*

Homotrema data (concentration [specimens per 1 cm^3], taphonomy [% abundance], and fragment size [% abundance]) for each collected sample. Corresponding geomorphic zone, elevation, and distance from shoreline are indicated. Table S1 is located within Aquila.

Table S2: *PAM cluster analysis*

Results of PAM cluster analysis for each combination of data (tests 1 – 7) for each collected sample. For each test, the average silhouette width and percent accuracy are indicated for scenarios involving two to six clusters. Table S1 is located within Aquila.

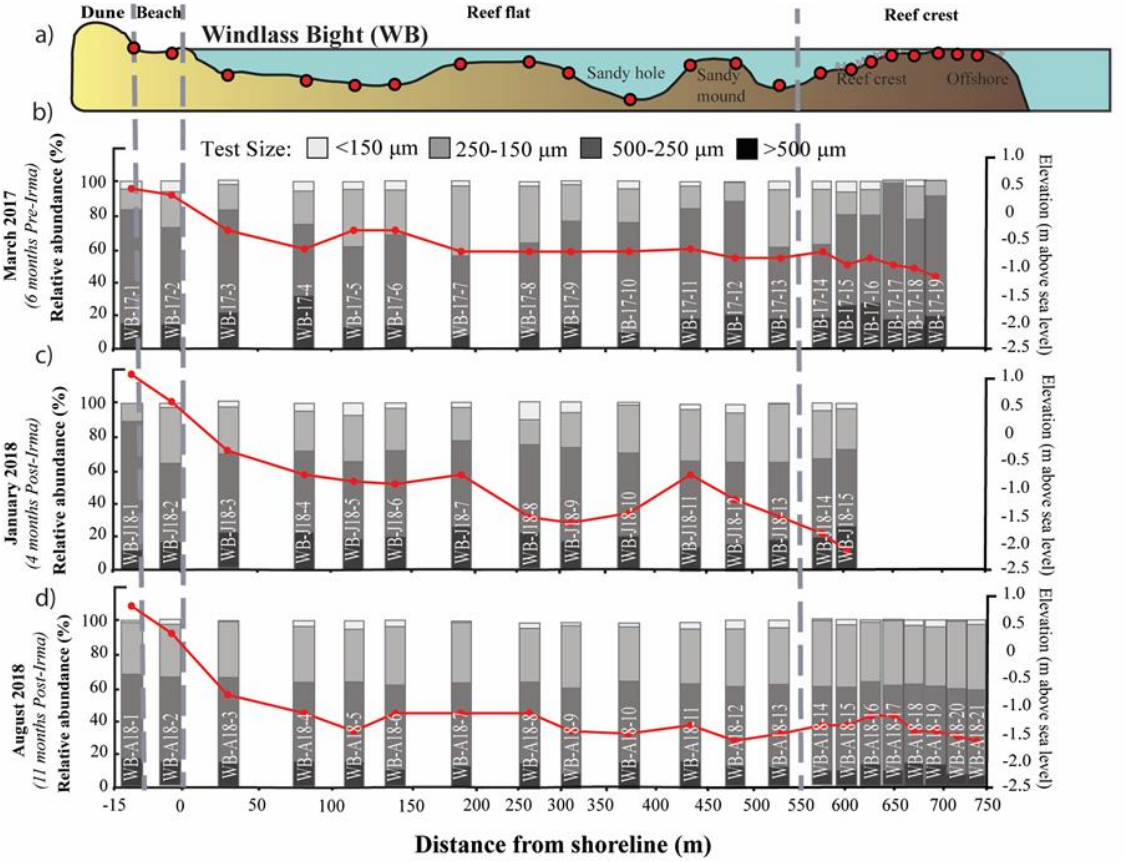

Figure S1: Windlass Bight fragment size

Homotrema fragment size distributions along the Windlass Bight (WB) transect (north side of Anegada) relative to increasing distance offshore. (a) Nearshore cross-section of WB indicating sample locations (red circles) and major geomorphic changes along transect. Relative abundances (%) of each size category (b – d) in each of the three sampling intervals. Corresponding surface elevation profiles indicated by a solid red line.

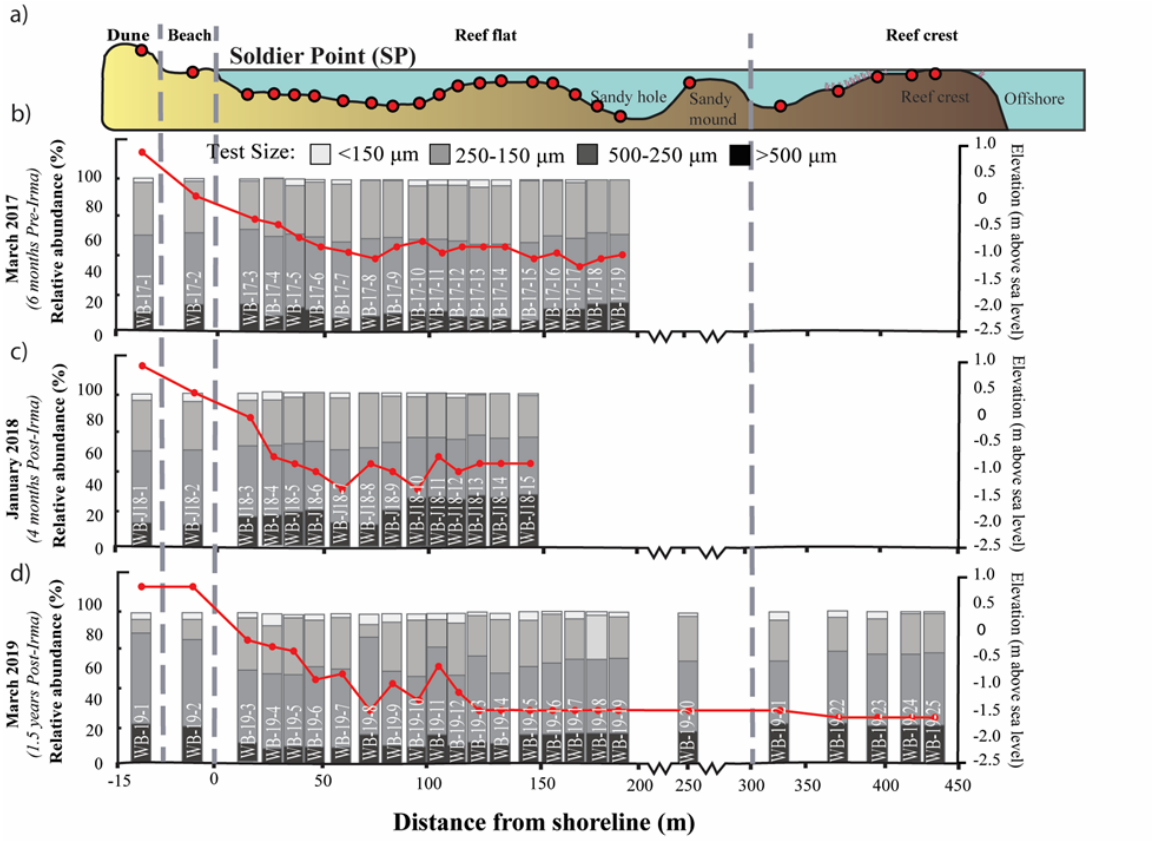

Figure S2: Soldier Point fragment size

Homotrema fragment size distributions along the Soldier Point (SP) transect (north side of Anegada) relative to increasing distance offshore. (a) Nearshore cross-section of SP indicating sample locations (red circles) and major geomorphic changes along transect. Relative abundances (%) of each size category (b – d) in each of the three sampling intervals. Corresponding surface elevation profiles indicated by a solid red line.

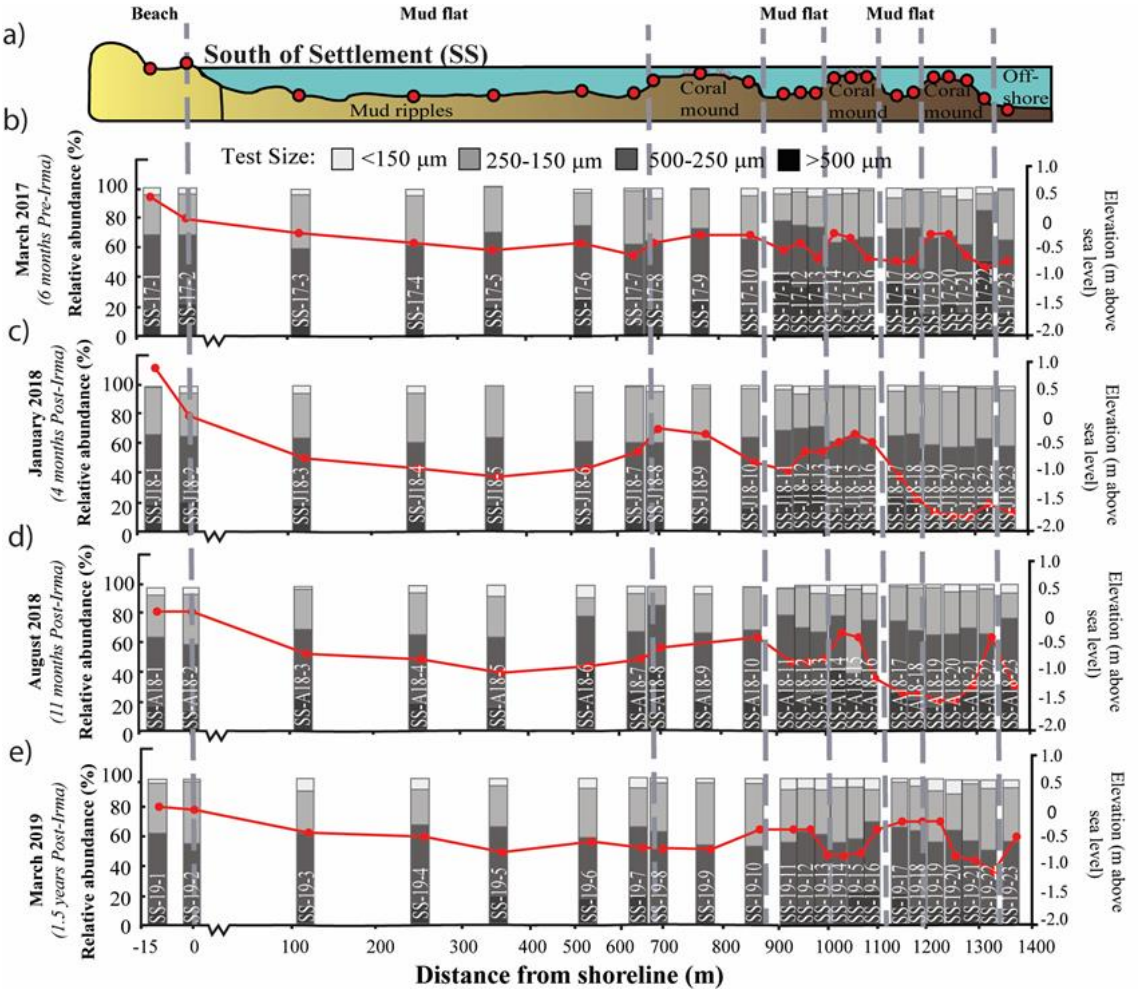

Figure S3: South of Settlement fragment size

Homotrema fragment size distributions along the South of Settlment (SS) transect (south side of Anegada) relative to increasing distance offshore. (a) Nearshore cross-section of SS indicating sample locations (red circles) and major geomorphic changes along transect. Relative abundances (%) of each size category (b – e) in each of the four sampling intervals. Corresponding surface elevation profiles indicated by a solid red line.

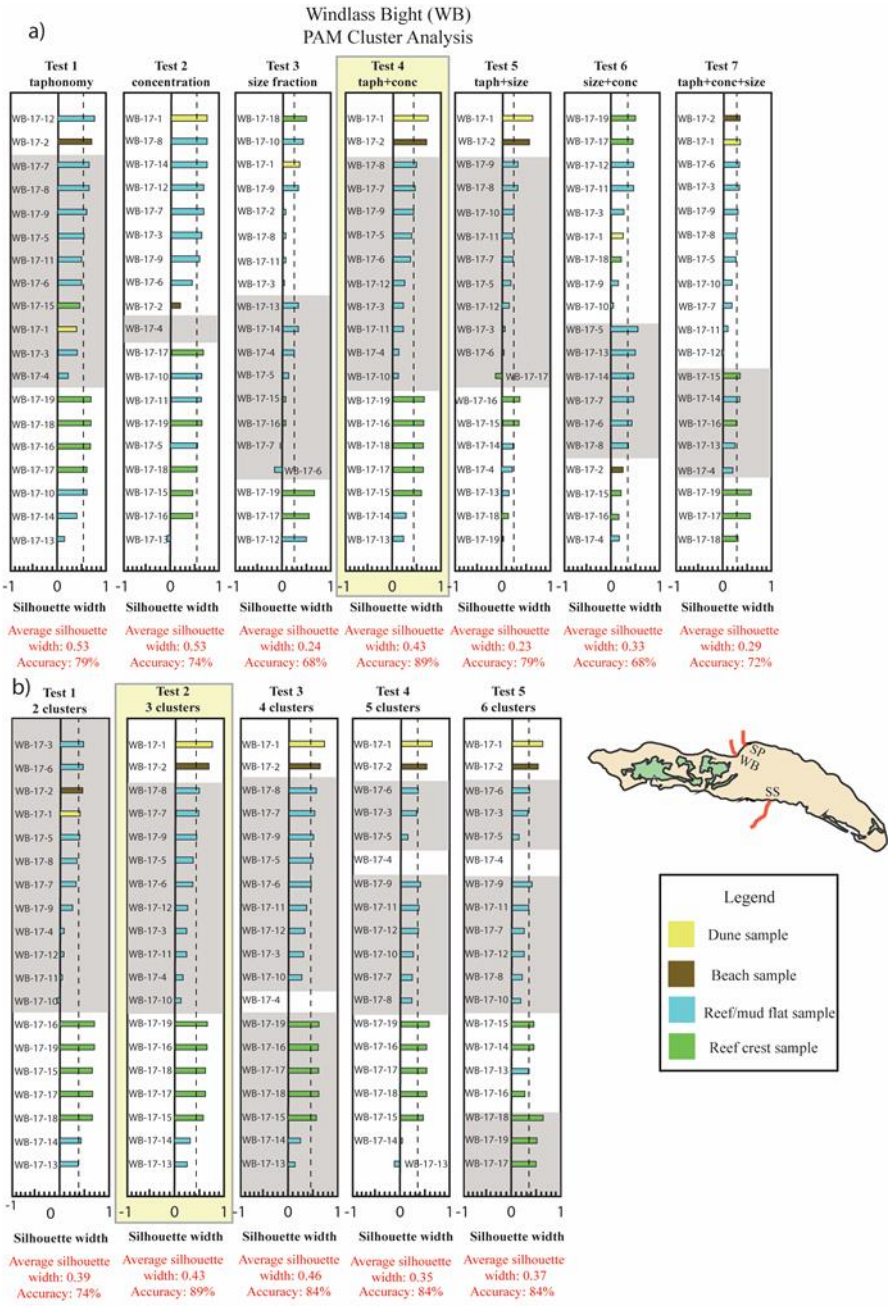

Figure S4: Windlass Bight PAM

Results of PAM cluster analysis for the Windlass Bight (WB) transect using pre-Hurricane Irma samples collected in March 2017. (a) Clustered data for tests 1 to 7 based on all possible data combinations (i.e., taphonomic, concentration, and test size data) showing that test 4 clusters data most appropriately (highlighted with yellow rectangle) based on its high average silhouette width (dashed line) and high percent accuracy value. (b) Using test 4 (a), five additional tests were run to determine that test 2 (3-cluster scenario) clustered pre-Hurricane Irma data (from March 2017) the most appropriately (highlighted with yellow rectangle).

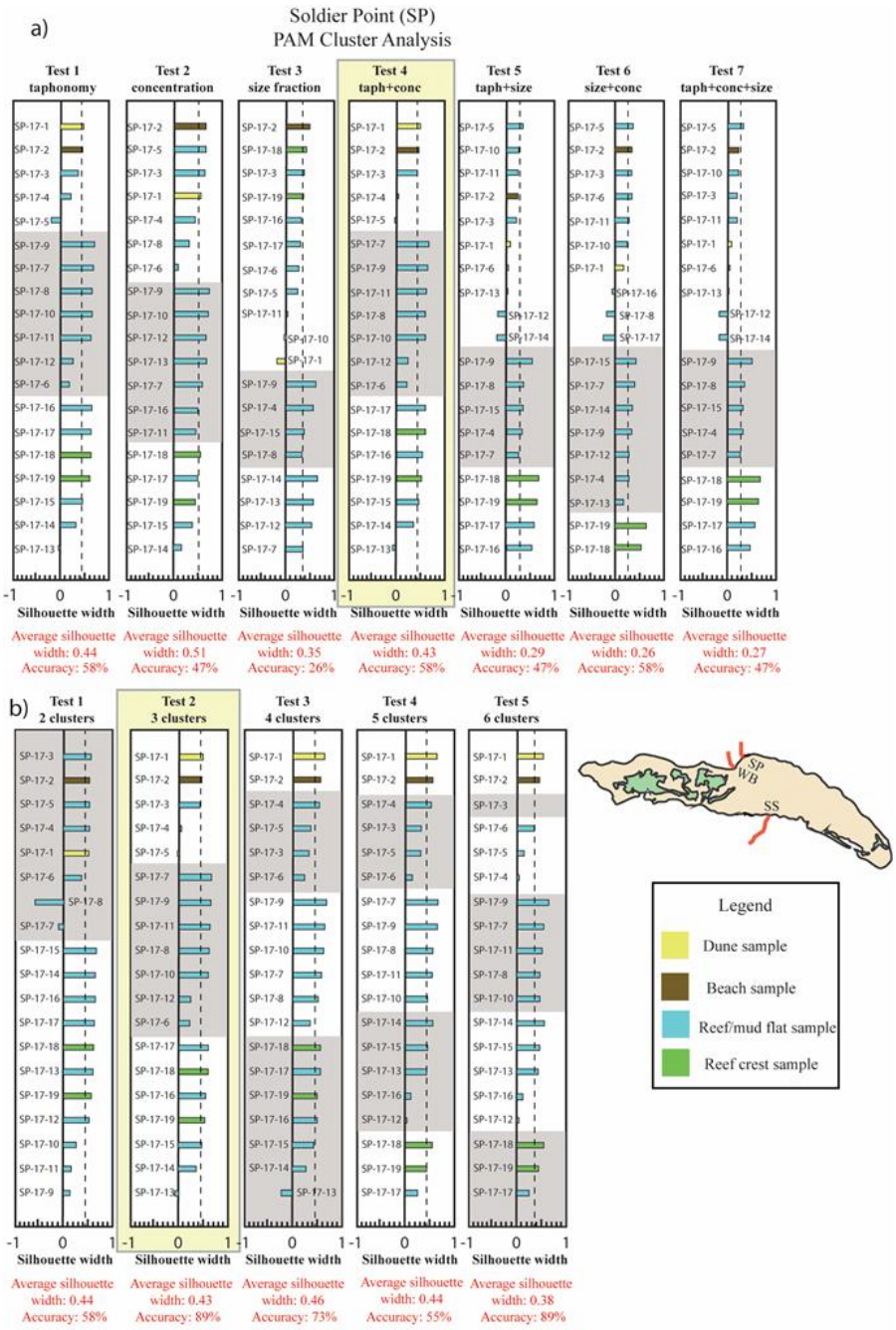

Figure S5: Soldier Point PAM

Results of PAM cluster analysis for the Soldier Point (SP) transect using pre-Hurricane Irma samples collected in March 2017. (a) Clustered data for tests 1 to 7 based on all possible data combinations (i.e., taphonomic, concentration, and test size data) showing that test 4 clusters data most appropriately (highlighted with yellow rectangle) based on its high average silhouette width (dashed line) and high percent accuracy value. (b) Using test 4 (a), five additional tests were run to determine that test 2 (3-cluster scenario) clustered pre-Hurricane Irma data (from March 2017) the most appropriately (highlighted with yellow rectangle).

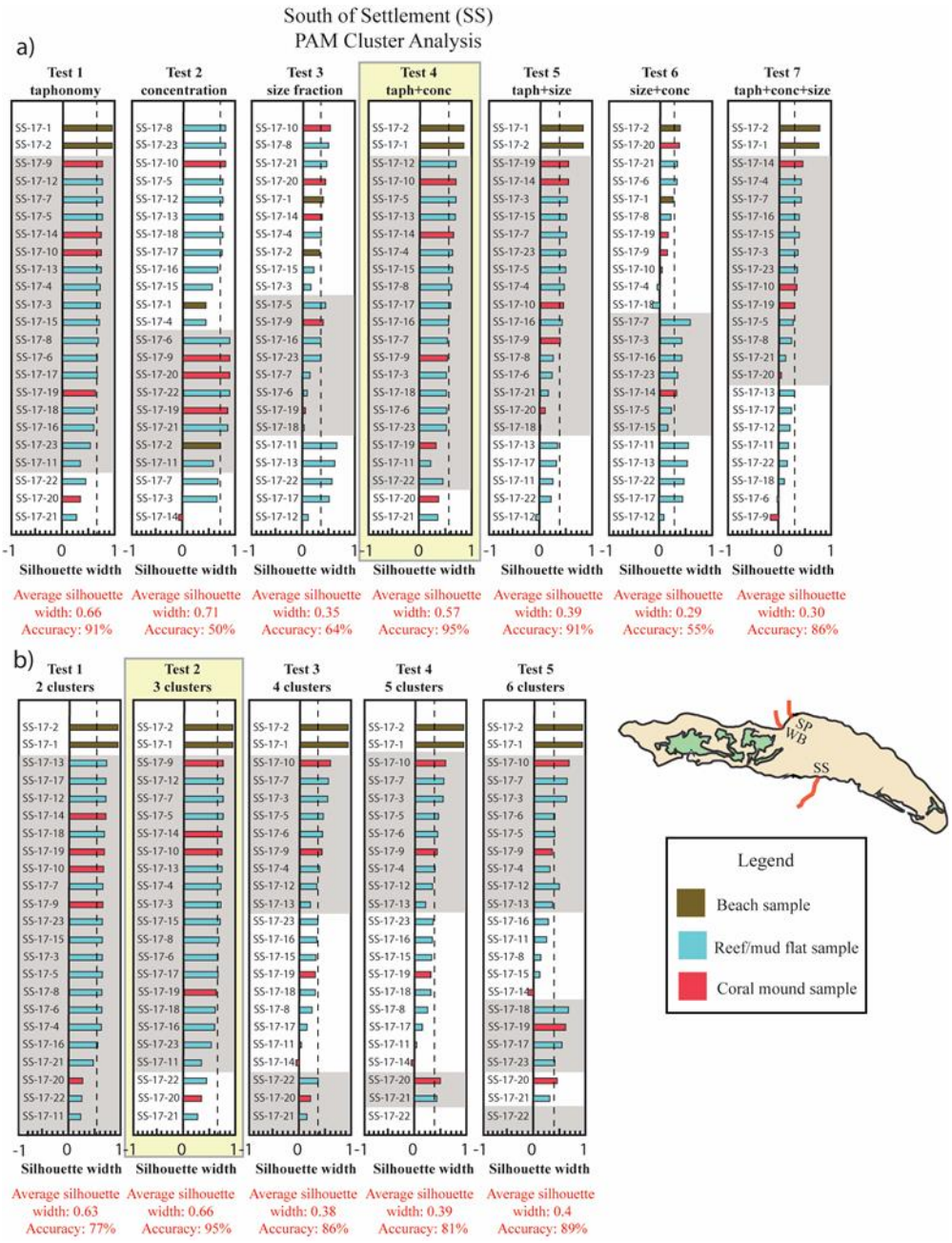

Figure S6: South of Settlement PAM

Results of PAM cluster analysis for the South of Settlement (SS) transect using pre-Hurricane Irma samples collected in March 2017. (a) Clustered data for tests 1 to 7 based on all possible data combinations (i.e., taphonomic, concentration, and test size data) showing that test 4 clusters data most appropriately (highlighted with yellow rectangle) based on its high average silhouette width (dashed line) and high percent accuracy value. b) Using test 4 from (a), five additional tests were run to determine that test 2 (3-cluster scenario) clustered pre-Hurricane Irma data (from March 2017) the most appropriately (highlighted with yellow rectangle).

REFERENCES

Alam, M., Zuraida, R., Yuliadi, L. S., Lili, W., Nurruhwati, I. *Homotrema rubrum* taphonomy as an indicator of sediment transport of the Bangka Island Waters, North Minahasa. *E&ES*, 176 (2018), pp. 012005.

Atwater, B. F., Uri, S., Buckley, M., Halley, R. S., Jaffe, B. E., López-Venegas, A. M., Reinhardt, E.G., Tuttle, M.P. Watt., S., Wei, Y. Geomorphic and stratigraphic evidence for an unusual tsunami or storm a few centuries ago at Anegada, British Virgin Islands. *Nat. Hazards*, *63* (2012), pp. 51-84.

Atwater, B. F., Fuentes, Z., Halley, R. B., Ten Brink, U. S., Tuttle, M. P. Effects of 2010 Hurricane Earl amidst geologic evidence for greater overwash at Anegada, British Virgin Islands. *Adv. Geosci*., *38* (2014), pp. 21-30.

Atwater, B. F., Uri, S., Cescon, A. L., Feuillet, N., Fuentes, Z., Halley, R. B., Nuñez, C., Reinhardt, E.G., Roger, J., Sawai, Y., Spiske, M., Tuttle, M.P., Wei, Y., Weil Accardo, J. Geologic evidence for catastrophic marine inundation in 1200–1480 CE near the Puerto Rico Trench at Anegada, British Virgin Islands. *Geosphere*, *13* (2017), pp. 301-368.

Bicchi, E., Debenay, J. P., Pages, J. Relationship between benthic foraminiferal assemblages and environmental factors in atoll lagoons of the central Tuamotu Archipelago (French Polynesia). *Coral Reefs*, *21* (2002), pp. 275-290.

Bregy, J. C., Wallace, D. J., Minzoni, R. T., Cruz, V. J. 2500-year paleotempestological record of intense storms for the northern Gulf of Mexico, United States. *Mar. Geol*., 396 (2018), pp. 26-42.

Cangialosi JP, Latto AS, Berg R. National Hurricane center tropical cyclone report: Hurricane Irma. Washington DC (2018). Available: https://www.nhc.noaa.gov/data/tcr/AL112017_Irma.pdf [Accessed 28 Nov 2019].

Culver, S. J., Twarog, M., Mallinson, D. J., Shazili, N. A. M., Buzas, M. A. Rapid Change of Foraminiferal Communities and Assemblages in the Setiu Estuary, Terengganu, Malaysia: Anthropogenic Drivers. *J. Foraminiferal Res,* 49 (2019), pp. 206-228.

Debenay, J. P. A guide to 1,000 foraminifera from Southwestern Pacific: New Caledonia. *IRD Editions* (2012).

Donato, S. V., Reinhardt, E. G., Boyce, J. I., Pilarczyk, J. E., Jupp, B. P. Particle-size distribution of inferred tsunami deposits in Sur Lagoon, Sultanate of Oman. *Mar. Geol., 257* (2009), pp. 54-64.

Dunn, G. E., Miller, B. I. The hurricane season of 1960. *Mon. Weather Rev*., 89 (1961), pp. 99- 108.

Dunne, R. P., Brown, B. E. Some aspects of the ecology of reefs surrounding Anegada, British Virgin Islands (1979). *Atoll res. bull*.

Dura, T., Hemphill-Haley, E., Sawai, Y., Horton, B. P. The application of diatoms to reconstruct the history of subduction zone earthquakes and tsunamis. *Earth Sci. Rev., 152* (2016), pp. 181-197.

Elsner, J. B. Continued Increases in the Intensity of Strong Tropical Cyclones. *Bull. Am. Meteorol. Soc.* (2020).

EMDAT: The International Disaster Database. Last accessed July 19, 2020. Available: http://www.public.emdat.be/index/.

Feldens, P., Schwarzer, K., Sakuna, D., Szczuciński, W., Sompongchaiyakul, P. Sediment distribution on the inner continental shelf off Khao Lak (Thailand) after the 2004 Indian Ocean tsunami. *Earth Planets Space, 64* (2012).

Gischler, E., Möder, A. Modern benthic foraminifera on Banco Chinchorro, Quintana Roo, Mexico. *Facies*, 55 (2009), pp. 27-35.

Hippensteel, S. P. and Martin, R. E. Foraminifera as an indicator of overwash deposits, barrier island sediment supply, and barrier island evolution: Folly Island, South Carolina. *Palaeogeogr. Palaeoclimatol. Palaeoecol*., 149 (1999), pp. 115-125.

Hippensteel, S. P., Garcia, W. J. Micropaleontological evidence of prehistoric hurricane strikes from southeastern North Carolina. *J. Coast. Res*., *30* (2014), pp. 1157-1172.

Horton, B. P., Rossi, V., Hawkes, A. D. The sedimentary record of the 2005 hurricane season from the Mississippi and Alabama coastlines. *Quat. Int*., 195 (2009), pp. 15-30.

Hong, I., Pilarczyk, J. E., Horton, B. P., Fritz, H. M., Kosciuch, T. J., Wallace, D. J., Dike, C., Rarai, A., Harrison, M.J., Jockley, F. R. Sedimentological characteristics of the 2015 tropical cyclone pam overwash sediments from Vanuatu, South Pacific. *Mar. Geol.*, *396* (2018), pp. 205-214.

Javaux, E. J., Scott, D. B. Illustration of modern benthic foraminifera from Bermuda and remarks on distribution in other subtropical/tropical areas. *Palaeontol. Electron*., 6 (2003), pp. 29.

Kaufman, L. and Rousseeuw, P. J. *Finding groups in data: an introduction to cluster analysis*. John Wiley & Sons, 344 (2009).

Kemp, A. C., Horton, B. P., Vann, D. R., Engelhart, S. E., Pre, C. A. G., Vane, C. H., Nikitina, D., Anisfeld, S. C. Quantitative vertical zonation of salt-marsh foraminifera for reconstructing former sea level; an example from New Jersey, USA. *Quat. Sci. Rev.*, *54* (2012), pp. 26-39.

Knapp, R.D., Rhome, J.R., Brown, D.P. National Hurricane center tropical cyclone report: Hurricane Katrina. Washington DC (2005). Updated September 14, 2011. Available: https://www.nhc.noaa.gov/data/tcr/AL122005_Katrina.pdf [Accessed 14 Jan 2020].

Kosciuch, T. J., Pilarczyk, J. E., Hong, I., Fritz, H. M., Horton, B. P., Rarai, A., Harrison, M.J., Jockley, F. R. Foraminifera reveal a shallow nearshore origin for overwash sediments deposited by Tropical Cyclone Pam in Vanuatu (South Pacific). *Mar. Geol.*, *396* (2018), pp. 171-185.

Lane, P., Donnelly, J. P., Woodruff, J. D., Hawkes, A. D. A decadally-resolved paleohurricane record archived in the late Holocene sediments of a Florida sinkhole. *Mar. Geol.*, *287* (2011), pp. 14-30.

Loeblich, A. R., Tappan, H. Foraminiferal genera and their classification. Van 664 Nostrand Rienhold Co., New York (1987).

Machado, A. J. and Moraes, S. S. A note on the occurrence of the encrusting foraminifera *Homotrema rubrum* in reef sediments from two distinctive hydrodynamic settings. *An. Acad. Bras. Ciênc*., *74* (2002), pp. 727-735.

MacKenzie, F. T., Kulm, L. D., Cooley, R. L., Barnhart, J. T. *Homotrema rubrum* (Lamarck), a sediment transport indicator. *J. Sediment. Res*., *35* (1965), pp. 265-272.

Maechler, M., Rousseeuw, P., Struyf, A., Hubert, M. Cluster analysis basics and extensions R Statistics Package (CRAN). (2005).

Mamo, B., Strotz, L., Dominey-Howes, D. Tsunami sediments and their foraminiferal assemblages. *Earth Sci. Rev., 96* (2009), pp. 263-278.

Martínez, M. L., Intralawan, A., Vázquez, G., Pérez-Maqueo, O., Sutton, P., Landgrave, R. The coasts of our world: Ecological, economic and social importance. *Ecol. Econ*., 63 (2007), pp. 254-272.

Milker, Y., Wilken, M., Schumann, J., Sakuna, D., Feldens, P., Schwarzer, K., Schmiedl, G. Sediment transport on the inner shelf off Khao Lak (Andaman Sea, Thailand) during the 2004 Indian Ocean tsunami and former storm events: evidence from foraminiferal transfer functions. *Nat. Hazards Earth Syst. Sci*., 13 (2013), pp. 3113-3128.

Millás, J. C., Pardue, L. Hurricanes of the Caribbean and adjacent regions, 1492-1800. Acad. Arts Sci. Am (1968).

Moreira, S., Costa, P. J., Andrade, C., Lira, C. P., Freitas, M. C., Oliveira, M. A., Reichart, G.J. High resolution geochemical and grain-size analysis of the AD 1755 tsunami deposit: Insights into the inland extent and inundation phases. *Mar. Geol., 390* (2017), pp. 94-105.

Nishijama, K., Mori, N., Yasuda, T., Shimura, T., Gogon, J., Gibson, D., Jockley, F. DPRI VMGD joint survey for Cyclone Pam damages, Port-Vila, Vanuatu (2015), [online]. Online: http://www.taifu.dpri.kyotou.ac.jp/wpcontent/uploads/2015/05/DPRIVMGD-survey-first-report-Final.pdf (accessed (07.02.20)).

Phalen, W. G., Bernhard, J. M., Bowser, S. S., Goldstein, S. T. Distribution, abundance, and laboratory calcification of *Homotrema rubrum* from Tennessee Reef, Florida Keys, USA. *J. Foramineferal Res*., 46 (2016), pp. 409-419.

Pham, D. T., Gouramanis, C., Switzer, A. D., Rubin, C. M., Jones, B. G., Jankaew, K., Carr, P. F. Elemental and mineralogical analysis of marine and coastal sediments from Phra Thong Island, Thailand: Insights into the provenance of coastal hazard deposits. *Mar. Geol., 385* (2017), pp. 274-292.

Pickering, V. W. Early history of the British Virgin Islands: from Columbus to emancipation. *Falcon Publications International* (1983).

Pilarczyk, J. E., Horton, B. P., Witter, R. C., Vane, C. H., Chagué-Goff, C., Goff, J. Sedimentary and foraminiferal evidence of the 2011 Tōhoku-oki tsunami on the Sendai coastal plain, Japan. *Sediment. Geol*., *282* (2012), pp. 78-89.

Pilarczyk, J. E., Dura, T., Horton, B. P., Engelhart, S. E., Kemp, A. C., Sawai, Y. Microfossils from coastal environments as indicators of paleo earthquakes, tsunamis and storms. *Palaeogeogr. Palaeoclimatol. Palaeoecol*., *413* (2014a), pp. 144-157.

Pilarczyk, J. E., Goff, J., Mountjoy, J., Lamarche, G., Pelletier, B., Horton, B. P. Sediment transport trends from a tropical Pacific lagoon as indicated by *Homotrema rubra* taphonomy: Wallis Island, Polynesia. *Mar. Micropaleontol*., *109* (2014b), pp. 21-29.

Pilarczyk, J. E., Horton, B. P., Soria, J. L. A., Switzer, A. D., Siringan, F., Fritz, H. M., Khan, N.S., Ildefonso, S.I., Doctor, A.A., Garcia, M. L. Micropaleontology of the

2013 Typhoon Haiyan overwash sediments from the Leyte Gulf, Philippines. *Sediment. Geol*., 339 (2016), pp. 104-114.

Pilarczyk, J. E., Sawai, Y., Matsumoto, D., Namegaya, Y., Nishida, N., Ikehara, K., Dura T., Horton, B. P. Constraining sediment provenance for tsunami deposits using distributions of grain size and foraminifera from the Kujukuri coastline and shelf, Japan. *Sedimentology*, 67 (2019), pp. 1373-1392.

Schomburgk, R. H. Remarks on Anegada. *J.R. Geog. Soc. Lon.*, 2 (1832), pp. 152-170.

Scott, D. B., Hermelin, J. O. R. (1993). A device for precision splitting of micropaleontological samples in liquid suspension. *J. Paleontol*., 67 (1993), pp. 151-154.

Seike, K., Shirai, K., Kogure, Y. Disturbance of shallow marine soft-bottom environments and megabenthos assemblages by a huge tsunami induced by the 2011 M9.0 Tohoku-Oki earthquake. *PLoS One*, *8* (2013), e65417.

Smedile, A., Molisso, F., Chagué, C., Iorio, M., De Martini, P. M., Pinzi, S., Collins, P.E.F., Sagnotti, L., Pantosti, D. New coring study in Augusta Bay expands understanding of offshore tsunami deposits (Eastern Sicily, Italy). *Sediment.*, 67 (2020), pp. 1553-1576.

So, S., Juarez, B., Valle-Levinson, A., Gillin, M. E. Storm surge from Hurricane Irma along the Florida Peninsula. *Estuarine Coastal Shelf Sci*., *229* (2019), pp. 106402.

Sobel, A. H., Camargo, S. J., Hall, T. M., Lee, C. Y., Tippett, M. K., Wing, A. A. Human influence on tropical cyclone intensity. *Science*, 353 (2016), pp. 242-246.

Soria, J. L. A., Switzer, A. D., Pilarczyk, J. E., Tang, H., Weiss, R., Siringan, F., Manglicmot, M., Gallentes, A., Annie Lau, A.Y., Cheong, A.Y.L., Koh, T. W. L.

Surf beat induced overwash during Typhoon Haiyan deposited two distinct sediment assemblages on the carbonate coast of Hernani, Samar, central Philippines. *Mar. Geol.*, *396* (2018), pp. 215-230.

Spiske, M., Halley, R. B. A coral-rubble ridge as evidence for hurricane overwash, Anegada (British Virgin Islands). Adv. Geosci., 38 (2014), pp. 9-20.

Strotz, L. C., Mamo, B. L., Dominey-Howes, D. Effects of cyclone-generated disturbance on a tropical reef foraminifera assemblage. *Sci. Rep*., *6* (2016), pp. 24846.

Sugawara, D., Goto, K., Imamura, F., Matsumoto, H., Minoura, K. Assessing the magnitude of the 869 Jogan tsunami using sedimentary deposits: Prediction and consequence of the 2011 Tohoku-oki tsunami. *Sed. Geol*., 282 (2012), pp. 14-26.

Toomey, M. R., Donnelly, J. P., Woodruff, J. D. Reconstructing mid-late Holocene cyclone variability in the Central Pacific using sedimentary records from Tahaa, French Polynesia. *Quat. Sci. Rev*., 77 (2013), pp. 181-189.

Tsuboki, K., Yoshioka, M. K., Shinoda, T., Kato, M., Kanada, S., Kitoh, A. Future increase of supertyphoon intensity associated with climate change. *Geophys. Res. Lett*., 42 (2015), pp. 646-652.

Watanabe, T., Tsuchiya, N., Yamasaki, S. I., Sawai, Y., Hosoda, N., Nara, F. W., Nakamura, T., Komai, T. A geochemical approach for identifying marine incursions: Implications for tsunami geology on the Pacific coast of northeast Japan. *Appl. Geochem*., 118 (2020), pp. 104644.

Woodruff, J. D., Irish, J. L., Camargo, S. J. Coastal flooding by tropical cyclones and sea level rise. *Nature*, 504 (2013), pp. 44-52.

Yannarell, A. C., Steppe, T. F., Paerl, H. W. Disturbance and recovery of microbial community structure and function following Hurricane Frances. *Environ. Microbiol*., 9 (2007), pp. 576-583.

Zahibo, N., Pelinovsky, E., Yalciner, A., Kurkin, A., Koselkov, A., Zaitsev, A. The 1867 Virgin Island tsunami: observations and modeling. *Acta Oceanolog*., 26 (2003), pp. 609-621.